

Taxonomy of groundwater quality using multivariate and spatial analyses in the Tuticorin District, Tamil Nadu, India

C. Singaraja¹ · S. Chidambaram² · Noble Jacob³ ·
E. Ezhilarasan¹ · C. Velmurugan¹ · M. Manikandan¹ ·
S. Rajamani¹

Received: 25 June 2014 / Accepted: 14 March 2015 / Published online: 25 March 2015
© Springer Science+Business Media Dordrecht 2015

Abstract A holistic appraisal of the quality of groundwater from the Tuticorin District has been conducted using multivariate statistical and spatial analyses. The objectives of the study were to delineate the spatial and temporal variabilities in groundwater quality and to understand its suitability for human uses. A total of 100 groundwater samples were collected and analyzed for major cations and anions during pre-monsoon and post-monsoon. Water quality index rating was calculated to quantify overall water quality for human consumption. The PRM samples exhibit poor quality in greater percentage when compared with POM due to the dilution after rainfall. Correlation, factor analysis, and plot of the factor scores reflect the seawater intrusion and weathering process. The mineral stability

✉ C. Singaraja
geolionking@gmail.com

S. Chidambaram
chidambaram_s@rediffmail.com

Noble Jacob
noblej@barc.gov.in

E. Ezhilarasan
ezhilan009geo@gmail.com

C. Velmurugan
velmurugan89@gmail.com

M. Manikandan
manikandanm880@gmail.com

S. Rajamani
rajamani303@gmail.com

¹ Department of Geology, Presidency College, Chennai 5, Tamil Nadu, India

² Department of Earth Sciences, Annamalai University, Annamalai Nagar 608002, India

³ Isotope Production and Applications Division, Bhabha Atomic Research Centre, Mumbai 400 085, India

diagrams indicated that the groundwater is in equilibrium with kaolinite and Ca-montmorillonite, whereas Gibbs plot showed that the chemical composition of groundwater in both districts is controlled by the natural weathering processes irrespective of seasons. The major water type identified in this study is the $\text{Ca}^{2+}\text{-Mg}^{2+}\text{-HCO}_3^-$ type, which degrades into predominantly $\text{Na}^+\text{-Cl}^-\text{-SO}_4^{2-}$ more saline groundwater toward the coast.

Keywords Multivariate statistics · Water quality index · Seawater intrusion · Weathering process

1 Introduction

In the Tuticorin District, attention on groundwater abstraction from the aquifers has increased during the last decade (Balasubramanian et al. 1993; Mondal et al. 2009, 2011; Singaraja et al. 2013a, b). This is due to rising water demands from an increasing population (Mondal et al. 2009; Soundranayagam et al. 2009). Salinization has been identified as a major problem affecting groundwater in the Tuticorin District (CGWB 2009; Singaraja 2015). A lot of potential sites for wells and boreholes were not completed due to salinity problems in the aquifers, and some obtainable deep wells and dug wells have been abandoned due to increasing salinity over time. Almost all communities in the basin have relied on groundwater from the perched shallow aquifers to meet both domestic and irrigation needs over the past years. However, sanitary conditions around the wellhead in most cases are very poor leading to contamination from surface sources.

The study area, Tuticorin District, a hard rock terrain receives major part of rainfall from northeast monsoon. The surface water sources generally get their supply during monsoon seasons, and during pre-monsoonal periods, people have to generally depend on groundwater resources for their domestic, agricultural, and industrial activities. About 70 % of study area is dominated by agricultural activities among other things, while the remaining parts of the area are dominated by industrial activities such as petrochemical production, thermal power plant, and fertilizer production among other things. These activities generate large hazards in the area and thereby create a major threat to groundwater. Salt is produced on a widespread scale in Tuticorin District; it constitutes 70 % of the total salt production of the state and meets almost 30 % of the requirement of the country. The salt pan area has increased at the expense of agricultural land, coastal sand with/without vegetation, sand dunes, scrub, and mudflats, and this has seriously affected the groundwater (Singaraja et al. 2014b). Such a study to identify the spatial variation in groundwater quality control parameters is necessary in order to delineate areas of extremely poor groundwater quality, for treatment before various uses.

In this study, multivariate statistical methods have been used jointly with predictable graphical methods, to study the causes of variation in the salinity and to spatially classify groundwater in the area. Groundwater electrical conductivity (EC) has been used as a measure of salinity since it provides a measure of the total dissolved ions in the groundwater system. Six indices such as sodium percentage (Na %), sodium adsorption ratio (SAR), residual sodium carbonate (RSC), magnesium hazard (MH), Kelly's ratio (KR), and Puri Salt Index (PSI) were then used to find out the suitability of groundwater from within the study area for irrigation activities.

2 Study area

The present study area is situated in the southeast coast of Tamil Nadu, India. It is located between $8^{\circ} 19'$ to $9^{\circ} 22'N$ latitude and $77^{\circ} 40'$ to $78^{\circ} 23'E$ longitude (Fig. 1) covering an area of about 4621 km^2 , which constitutes 462 villages. The population is about 1,572,273, which largely depends on irrigation. The area experiences a hot tropical climate. The average annual temperature is 23 to 29°C , and the annual rainfall is about 570 to 740 mm . The district receives rain under the influence of both southwest and north-east monsoons. The north-east monsoon chiefly contributes to the rainfall in the district.

Geologically three major units exist in this area, hornblende biotite gneiss (HBG), alluvial marine, and fluvial marine (Fig. 1). The HBG is the dominant formation, and however, alluvial deposits occur on both sides of the river, which are composed of clay, silt, sand, and gravel. Alluvial marine and fluvial marine are dominant in the eastern part of the study area. Charnockite patches are noted in the central part as well as along the western margin of the study area. The study area is also represented by intrusions of granite, quartzite, and patches of sandstone. Major water-bearing formations are Quaternary alluvium, Tertiary formations, weathered fractured pink granites, charnockites, and gneisses. Limited freshwater availability is noted in sedimentary areas, and the floating lenses of freshwater make the coastal area vulnerable for water quality changes. Groundwater from alluvial/tertiary aquifer present in eastern part of the district is in hydraulic connection with the sea, and hence, it is vulnerable to saline water intrusion (CGWB 2009; Singaraja 2014).

3 Materials and methods

A total of 100 groundwater samples (Fig. 1) were collected during PRM and POM (2013). The sample bottles were labeled, sealed, and transported to the laboratory under standard preservation methods. The major anionic and cationic concentrations were determined in the

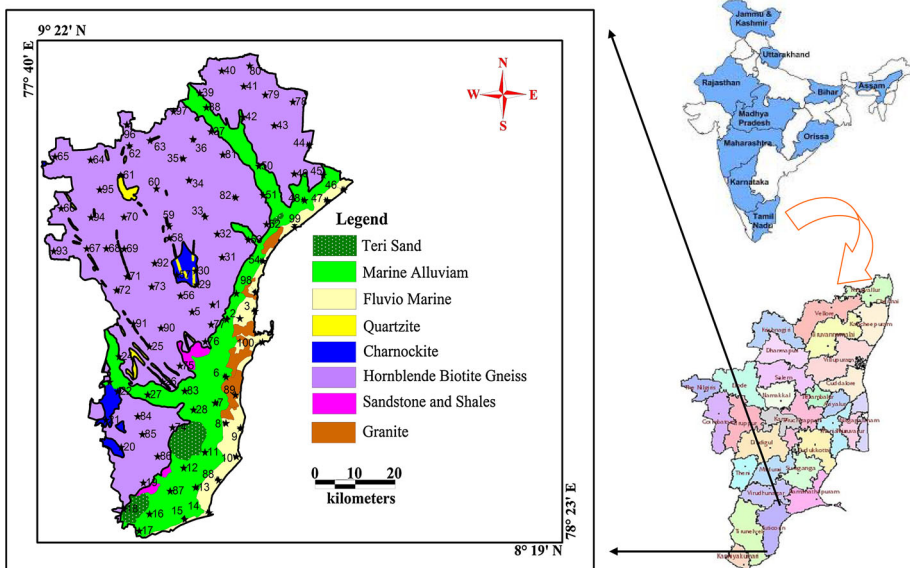


Fig. 1 Sampling location and geology map of the study area

laboratory using the standard analytical procedures (Table 1) as recommended by the American Public Health Association (1995). EC, pH, and temperature were measured directly in the field. Samples for laboratory analysis were immediately filtered in the field through 0.45-micron cellulose membranes. Na^+ and K^+ were determined by using flame photometer (Model, CL-361 Elico limited, Hyderabad, India). Ca^{2+} , Mg^{2+} , Cl^- , and HCO_3^- were determined by volumetric titration methods. Concentrations of SO_4^{2-} , H_4SiO_4 , and PO_4^- were determined by using UV–Vis double-beam spectrophotometry, Model SL 164 (Elico Limited, Hyderabad, India). Sulfate was estimated by common turbidity method using conditioning reagent (Glycerol + HCl + Ethyl alcohol), and by adding BaCl_2 , the turbidity was measured at 420 nm, phosphate by orthophosphate method at 880 nm, and dissolved silica was analyzed by molybdsilicate method at 810 nm. Fluoride was analyzed by using portable Thermo Orion ion electrode meter by using buffer solution (TISAB III). Analytical grade chemicals were used throughout the study without further purification. All reagents and

Table 1 Instrumental and volumetric methods used for chemical analysis of groundwater in the study area

Chemical parameter	Units	Method, instrument (make)	Reagents (make)	Reference
pH		pH meter (Systronics)	pH 4, 7, and 9.2 (buffer solutions)	APHA (1995)
EC	$\mu\text{S cm}^{-1}$	EC meter(Systronics)	Potassium chloride (Rankem)	APHA (1995)
TDS	mg l^{-1}	TDS meter (Hanna)		
Ca^{2+}	mg l^{-1}	EDTA titrimetric	EDTA, sodium hydroxide, and murexide (Rankem)	APHA (1995)
Mg^{2+}	mg l^{-1}	EDTA titrimetric	EDTA, sodium hydroxide, ammonia buffer, and Eriochrome black-T (Rankem)	APHA (1995)
Na^+	mg l^{-1}	Flame photometer (Elico)	Sodium chloride (NaCl), KCl, and calcium carbonate (CaCO_3) (Rankem)	APHA (1995)
K^+	mg l^{-1}	Flame photometer (Elico)	NaCl, KCl, and CaCO_3 (Rankem)	APHA (1995)
HCO_3^-	mg l^{-1}	Titrimetric	Hydrosulfuric acid (H_2SO_4), phenolphthalein, and methyl orange (Rankem)	APHA (1995)
Cl^-	mg l^{-1}	Titrimetric	Silver nitrate, potassium chromate (Rankem)	APHA (1995)
SO_4^{2-}	mg l^{-1}	UV–Vis double-beam spectrophotometer(Elico)	Glycerol, HCl, ethyl alcohol, NaCl, barium chloride, sodium sulfate (Rankem)	APHA (1995)
NO_3^-	mg l^{-1}	Spectrophotometer (Systronics)	Brucine–sulfanilic acid, potassium nitrate, and H_2SO_4 (Rankem)	APHA (1995)
F^-	mg l^{-1}	Ion electrode (Thermo Orion)	F 4, 7, and 9.2 (buffer solutions) (TISAB III) (Rankem)	APHA (1995)
H_4SiO_4	mg l^{-1}	UV–Vis double-beam spectrophotometer(Elico)	H_2SO_4 , ammonium molybdate, sodium hydroxide, oxalic acid, ascorbic acid, sodium metasilicate (Rankem)	APHA (1995)
PO_4^-	mg l^{-1}	UV–Vis double-beam spectrophotometer(Elico)	H_2SO_4 , potassium antimony tartrate, ammonium molybdate, ascorbic acid, potassium dihydrogen phosphate (Rankem)	APHA (1995)

calibration standards were prepared using double distilled water. The accuracy of complete chemical analysis of a groundwater sample was checked by computing the cation–anion balance (Eq. 1), where the total concentrations of cations, $\text{Ca}^{2+} + \text{Mg}^{2+} + \text{Na}^+ + \text{K}^+$ (TCC) in milliequivalents per liter, should be equal to the total concentrations of anions, $\text{HCO}_3^- + \text{Cl}^- + \text{SO}_4^{2-} + \text{NO}_3^- + \text{F}^-$ (TCA), expressed in the same units.

$$\text{cation–anion balance} = \frac{[(\text{TCC} - \text{TCA}) / (\text{TCC} + \text{TCA})] \times 100}{(1)} \quad (1)$$

The reaction (cationic and anionic balance) errors (E) of all the groundwater samples were within the acceptable limit of $\pm 10\%$, an added proof for the precision of the data (Mathess 1982; Domenico and Schwartz 1990). Mapinfo Software version 8 and Vertical mapper were used for the generation of spatial distribution maps. Aquachem Software version 4 was used for Wilcox (1955) diagram, WATQ4F software was used for thermodynamic stability diagram, and SPSS Statistic Software version 17 was used for correlation.

4 Results and discussion

4.1 Hydrogeochemistry

The water pH cut across both acidic and alkaline in nature in most samples ranges between 6.80–9.20 and 6.80–9.40 during PRM and POM seasons, respectively (Table 2). The TDS, which indicates total dissolved solids in the water, range between 194.50 and 16,685.61 mg l^{-1} during PRM and 300 and 12,727 mg l^{-1} during POM, respectively. EC measures of charged ions in groundwater range between 308.80–28140 $\mu\text{S cm}^{-1}$ in PRM and 461–19872 $\mu\text{S cm}^{-1}$ in POM.

Ca^{2+} concentration ranges from 4 to 1600 mg l^{-1} during PRM and from 29 to 500 mg l^{-1} during POM. The concentration of magnesium in groundwater samples in the study area varies from 4.80 to 1248 mg l^{-1} and 9 to 895 mg l^{-1} during PRM and POM, respectively. Higher Ca^{2+} and Mg^{2+} were noted in PRM compared to POM. In many locations, $\text{Mg}^{2+} > \text{Ca}^{2+}$, this may be due to the influence of seawater intrusion (Mondal et al. 2008). Na^+ concentration varies from 14.80 to 4488 mg l^{-1} and 4 to 4250 mg l^{-1} during PRM and POM. Sodium concentration also exceeds permissible limit, and the increasing sodium in groundwater is likely due to seawater influence or salt pan deposits or ionic exchange process. In contrast to the concentrations of Ca^{2+} , Mg^{2+} , and Na^+ ions among the cations, the lower concentration of K^+ is observed between 0.5 and 520 mg l^{-1} during PRM and 2 and 213 mg l^{-1} during POM from the groundwater, because the potash feldspars are more resistant to chemical weathering and are fixed on clay products.

Cl^- is derived mainly from the non-lithological source, and its solubility is generally high. It ranges from 35.45 to 10,812.25 mg l^{-1} during PRM and 35.45 to 9052.50 mg l^{-1} during POM. Higher concentration of chloride in the coastal region may be due to seawater intrusion (Chidambaram et al. 2007; Singaraja et al. 2012; Khaska et al. 2013; Warner et al. 2013) and also may be due to leaching from upper soil layers derived from industrial and domestic activities (Srinivasamoorthy et al. 2008). The value of HCO_3^- ranges from 12.2 to 536 mg l^{-1} during PRM and 50.4 to 683 mg l^{-1} during POM, respectively. The higher concentration of HCO_3^- in the water reflects mineral dissolution result from high weathering process (Stumm and Morgan 1996). SO_4^{2-} values range from 0.50 to 456 mg l^{-1} and 2 to 312 mg l^{-1} during PRM and POM, and higher sulfate noted in PRM

Table 2 Maximum, minimum, and average of the chemical constituents in groundwater representing all four seasons (all values in mg l^{-1} except EC in $\mu\text{S cm}^{-1}$ and pH)

	Temp ($^{\circ}\text{C}$)	pH	TDS	EC	Ca^{2+}	Mg^{2+}	Na^{+}	K^{+}	F^{-}	Cl^{-}	HCO_3^{-}	NO_3^{-}	PO_4^{-}	SO_4^{2-}	H_4SiO_4
Pre-monsoon															
Avg	32.35	7.57	1843.33	2878.23	100.54	78.62	424.56	45.55	0.53	922.83	160.95	7.02	0.62	72.55	61.75
Max	35.90	9.20	16731.21	26240.00	1600.00	1248.00	3980.00	520.50	3.30	10812.25	536.80	148.00	12.00	456.00	125.00
Min	27.60	6.80	204.62	308.80	4.00	4.80	14.80	0.50	BDL	35.45	12.20	0.51	BDL	1.00	1.25
Post-monsoon															
Avg	31.82	7.67	1484.23	2357.86	81.37	50.04	365.27	25.42	0.46	636.04	338.88	4.34	0.21	37.78	12.21
Max	35.80	8.80	19365.68	30200.00	608.00	559.20	6812.00	218.50	2.43	10989.50	2940.20	57.00	3.21	324.00	15.20
Min	29.30	6.95	253.92	372.00	4.00	2.40	14.70	0.83	BDL	35.45	36.60	0.23	BDL	1.00	2.00

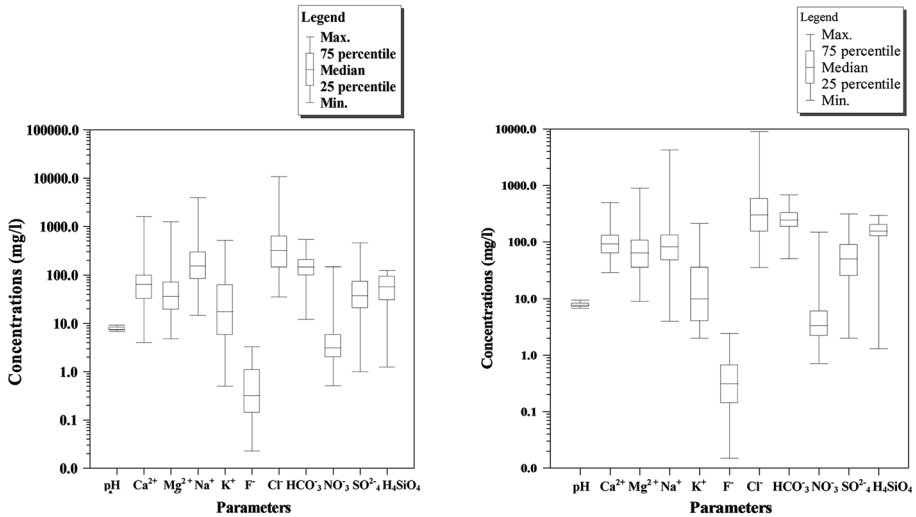


Fig. 2 Box plot for the maximum, minimum, and average of the chemical constituents in groundwater during PRM and POM (all values in mg l^{-1} except pH)

may be due to salt pans/seawater intrusion (Barbecot et al. 2000). The value of NO_3^- in the groundwater is observed to be between 0.51 and 148 mg l^{-1} and 0.7 and 148.20 mg l^{-1} during PRM and POM, respectively. Nitrate in groundwater is mainly derived from organic materials, industrial effluents, fertilizer, fixing bacteria, leaching of animal dung, sewage, and septic tanks (Richard 1954). The PO_4^{3-} concentration was found to be low in both the seasons BDL to 12.00. The results also show higher concentration of F^- (3.2 mg l^{-1}) during PRM compared to POM. Perhaps, due to the dilution effect, a similar trend was observed in Krishnagiri region (Manikandan et al. 2012).

The geochemical trend of groundwater in the study area (Fig. 2) demonstrates that sodium is the dominant cation ($\text{Na}^+ > \text{Ca}^{2+} > \text{Mg}^{2+} > \text{K}^+$). In majority of the samples, Na^+ , Mg^{2+} , and K^+ are above the median level based on whisker plot, and then, in Ca^{2+} , majority of the samples fall between median to minimum level. Similarly, chloride was found to be the dominant anion ($\text{Cl}^- > \text{HCO}_3^- > \text{SO}_4^{2-} > \text{H}_4\text{SiO}_4 > \text{NO}_3^- > \text{F}^-$). Cl^- , NO_3^- , and SO_4^{2-} in most of the samples fall within median to maximum level, and HCO_3^- , F^- , and H_4SiO_4 in majority of the samples lie between the median to maximum in anion during PRM. Na^+ , Mg^{2+} , and Ca^{2+} show uniform distribution of all the samples between minimum to maximum, but in K^+ most of the samples falls above the median in cation ($\text{Na}^+ > \text{Mg}^{2+} > \text{Ca}^{2+} > \text{K}^+$). Cl^- , NO_3^- , F^- , and H_4SiO_4 show most of the samples falls above the median to maximum level of the whisker plot, while in SO_4^{2-} majority of the samples lie between the median to minimum ($\text{Cl}^- > \text{HCO}_3^- > \text{SO}_4^{2-} > \text{H}_4\text{SiO}_4 > \text{NO}_3^- > \text{F}^-$) during POM.

4.2 Gibbs diagram

The Gibbs diagram is generally used to establish the relationship of water composition and aquifer lithological characteristics (Gibbs 1970). Three distinct fields such as precipitation dominance, evaporation dominance, and rock–water interaction dominance areas are shown in the Gibbs diagram (Fig. 3). The chemical composition of groundwater indicates the rock–water interaction (Elango and Kannan 2007). The groundwater samples from

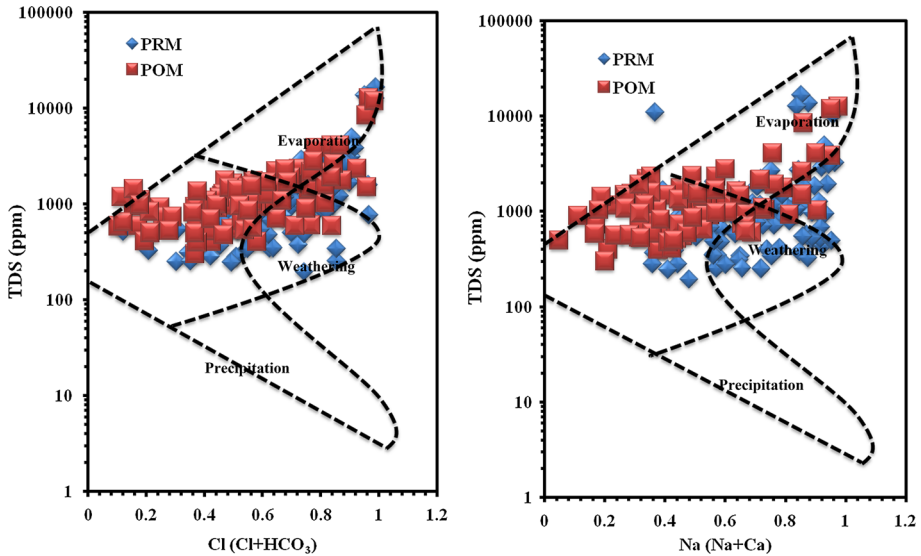


Fig. 3 Gibbs plot depicting the mechanism controlling the groundwater chemistry of different seasons

Tuticorin District during PRM and POM seasons fall in both weathering (the rock–water interaction) dominance and evaporation dominance field (Chowdhury and Gupta 2011). The majority of the samples during both seasons in the cation and anion plot fall in the rock weathering zone, and few samples represented in both plots fall in evaporation zone during both seasons in the study area. Evaporation greatly increases the concentrations of ions formed by chemical weathering, leading to higher salinity. A high level of evaporation can also increase the salinity and the relative proportion of Na^+ to Ca^{2+} (Gibbs 1970).

4.3 Piper diagram

Hill Piper plot (Piper 1953) is used to infer hydrogeochemical facies of groundwater (Fig. 4). In PRM, samples are clustered in the fields of 1, 2, 3, 4, and 5, and the majority of the samples are concentrated in the $\text{Na}^+ - \text{Cl}^-$ type, indicating the saline nature in the groundwater (Prasanna et al. 2010; Singaraja et al. 2013a) with minor representations from mixed $\text{Ca}^{2+} - \text{Mg}^{2+} - \text{Cl}^-$, mixed $\text{Ca}^{2+} - \text{Na}^+ - \text{HCO}_3^-$, $\text{Ca}^{2+} - \text{Cl}^-$, and $\text{Ca}^{2+} - \text{HCO}_3^-$ types. From the plot, alkalis (Na and K) exceed alkaline earths (Ca^{2+} and Mg^{2+}) and strong acids (Cl^- and SO_4^{2-}) exceed weak acid (HCO_3^-). In the groundwater of $\text{Na}^+ - \text{Cl}^-$ type, Na^+ is considered to be derived from mixing with seawater. The dominance of Na^+ in this water could also be caused by the water's increased alteration capacity due to the high CO_3 concentration that favors the solubility of alkaline elements from silicic rocks. Hence, increase in Na^+ is also attributable to seawater intrusion/dissolution of sodium-rich feldspars. However, ion exchange phenomena between Na^+ and Ca^{2+} could also be responsible for sodium and calcium concentrations (Lambrakis and Kallergis 2005) or due to seawater intrusion (Chidambaram et al. 2007).

In POM, samples are clustered in the fields of 1, 2, 3, 4, and 5, and the majority of the samples are concentrated in the $\text{Ca}^{2+} - \text{Mg}^{2+} - \text{Cl}^-$ type and mixed $\text{Ca}^{2+} - \text{Cl}^-$ type. Ca and Mg are major cations, and Cl^- is the major anion in this groundwater. These facies are

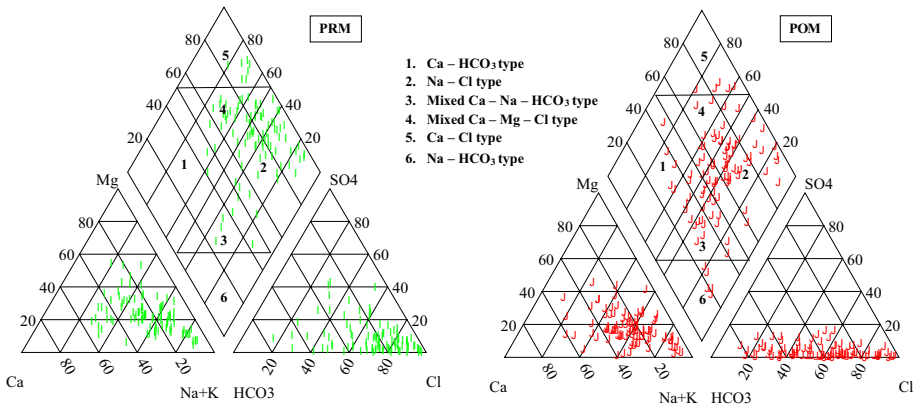


Fig. 4 Piper facies diagram for groundwater samples representing PRM and POM

characterized by low concentration of HCO_3^- and relatively higher concentration of Cl^- and Ca^{2+} , which are mainly distributed among the marine sediments and occur in the intermediate zone of groundwater discharge area where a similar trend was observed in Cuddalore District (Prasanna et al. 2010). It is also observed from the Piper plot that certain groundwater samples also show that alkaline earths (Ca^{2+} and Mg^{2+}) exceed the alkalis (Na^+ and K^+) and the strong acids (SO_4^{2-} and Cl^-) exceed the weak acids (HCO_3^-) (Udayalaxmi et al. 2010), and $\text{Ca}^{2+}\text{-Cl}^-$ type water may be a leading edge of the seawater plume (Appelo and Postma 1999; Jeen et al. 2001). Few samples represented the fields 1 and 2. From the plot, it is clearly evident that strong seawater influence in PRM when compared to POM which indicate clear shift from $\text{Ca}^{2+}\text{-HCO}_3^-$ to $\text{Na}^+\text{-Cl}^-$ type. (Rasouli and Masoudi 2012).

4.4 $\text{Cl}^-/\text{HCO}_3^-$ ratio

Chloride is the dominant ion found in seawater, while bicarbonate is present only in very small amounts; the chloride to total carbonate (carbonate + bicarbonate) is known as Simpson's ratio (Todd 1959). It is important in detecting seawater polluting the freshwater.

Simpson classification includes five classes: <0.5 for good-quality water, $0.5\text{--}1.3$ for slightly contaminated water, $1.3\text{--}2.8$ for moderately contaminated water, $2.8\text{--}6.6$ for injuriously contaminated water, and >15.5 for highly contaminated water. Considering the threshold value of Cl^- concentration (63 mg l^{-1}) and the ratio of $\text{Cl}^-/\text{HCO}_3^-$, it was found that about 32 and 12 % of the groundwater samples were strongly affected by the saline water during PRM and POM. 56 and 29 % were slightly or moderately affected during POM and PRM season, respectively (Fig. 5). 35 and 12 % of the samples fall on injuriously contaminated by seawater region during both seasons. 15 and 4 % of samples were not affected by seawater during POM and PRM, respectively.

The ratios of $\text{Cl}^-/\text{HCO}_3^-$ ranged between 0.14 and 152.50 and had strong positive linear relation with Cl^- concentrations with R^2 value of 0.92 (Fig. 5). This linear relationship indicates simple mixing of fresh groundwater with saline waters. It is also interesting to note that there is slight deviation in the linear relationship at the lower range of the mole ratios; this is mainly due to the variation in the HCO_3^- values. The decrease in this HCO_3^- ion represents in the increase in the $\text{Cl}^-/\text{HCO}_3^-$ ratio even at the lower values

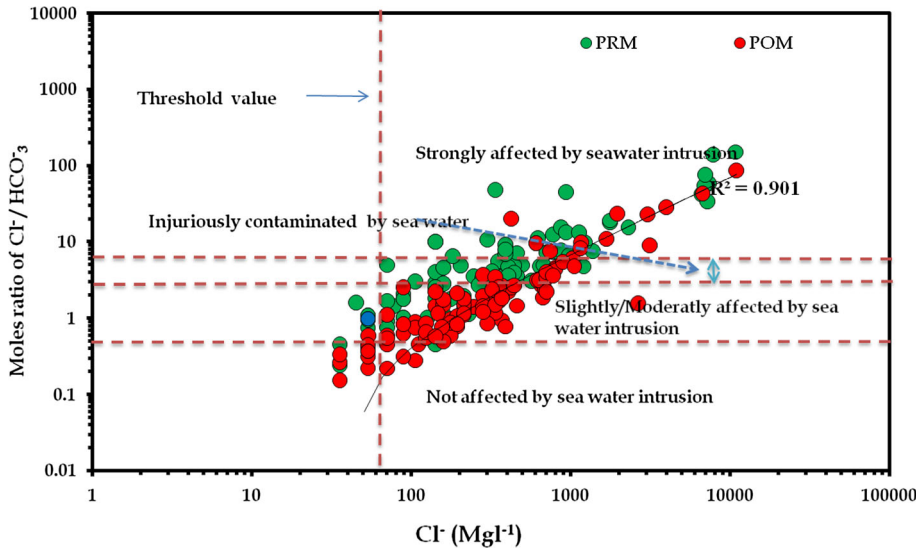


Fig. 5 Molar ratios of $\text{Cl}^-/\text{HCO}_3^-$ versus Cl^- concentration during PRM and POM seasons

of the Cl^- represented in the “X-” axis. This decrease in HCO_3^- value or increase in Cl^- relative to HCO_3^- ions is mainly due to land-use pattern (percolation of salt pans/industrial effluents) along the coast.

4.5 Chadha plot

A hydrochemical diagram proposed by (Chadha 1999) has been applied in this study to interpret the hydrochemical processes occurring in the study area. The same procedure was successfully applied by (Vandenbohede et al. 2010; Singaraja et al. 2013a) in a coastal aquifer to determine the evolution of two different hydrogeochemical processes. Data were converted to percentage reaction values (milliequivalent percentages) and expressed as the difference between alkaline earths ($\text{Ca}^{2+} + \text{Mg}^{2+}$) and alkali metals ($\text{Na}^+ + \text{K}^+$) for cations, and the difference between weak acidic anions ($\text{HCO}_3^- + \text{CO}_3$) and strong acidic for anions ($\text{Cl}^- + \text{SO}_4^{2-}$). The hydrochemical processes suggested by Chadha (1999) are indicated in each of the four quadrants of the graph.

These are broadly summarized as:

- Field 5: Ca^{2+} - HCO_3^- type recharging waters
- Field 6: Ca^{2+} - Mg^{2+} - Cl^- type reverse ion exchange waters
- Field 7: Na^+ - Cl^- type end-member waters (seawater)
- Field 8: Na^+ - HCO_3^- type base ion exchange waters

The Chadha’s diagram is exhibited in Fig. 6. Field 5 (recharging water): when water enters into the ground from the surface, it carries dissolved carbonate in the form of HCO_3^- and the geochemically mobile Ca^{2+} . Field 6 (reverse ion exchange): waters are less easily defined and less common, but represent groundwater where $\text{Ca}^{2+} + \text{Mg}^{2+}$ is in excess to $\text{Na}^+ + \text{K}^+$ either due to the preferential release of Ca^{2+} and Mg^{2+} from mineral weathering of exposed bedrock or possibly reverse base cation exchange reactions of

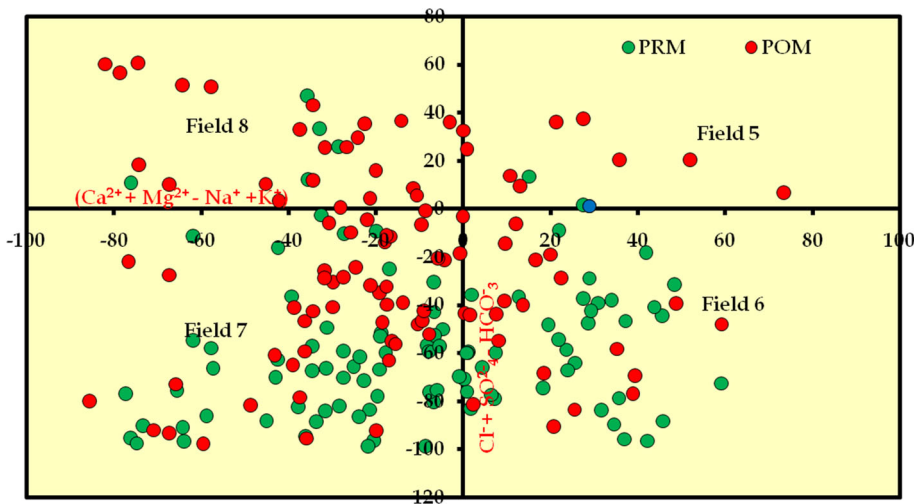


Fig. 6 Chadha's geochemical process evaluation for groundwater samples during PRM and POM seasons

$\text{Ca}^{2+} + \text{Mg}^{2+}$ into solution and subsequent adsorption of Na^+ on mineral surfaces. Field 7 ($\text{Na}^+ - \text{Cl}^-$): waters are typical seawater mixing and are mostly constrained to the coastal areas. Field 8 ($\text{Na}^+ - \text{HCO}_3^-$): waters possibly represent base exchange reactions or an evolutionary path of groundwater from $\text{Ca}^{2+} - \text{HCO}_3^-$ type freshwater to $\text{Na}^+ - \text{Cl}^-$ mixed seawater, where $\text{Na}^+ - \text{HCO}_3^-$ is produced by ion exchange processes. The plot shows that majority of samples of study area fall in Fields 6 and 7 (reverse ion exchange and seawater intrusion type) during PRM compared to POM may be due to the dilution effect after monsoon. Few groundwater samples fall in Field 8, indicating base exchange during both seasons, respectively. Very few samples fall in the recharge region during POM season. It is interesting to note that greater impact of seawater intrusion during PRM compared to POM season is noted in the Coastal region than in other parts of study area.

4.6 Correlation

In PRM, high positive correlation (>5) has been obtained between $\text{Cl}^- - \text{Ca}^{2+}$, $\text{Cl}^- - \text{Mg}^{2+}$, $\text{Cl}^- - \text{Na}^+$, $\text{Cl}^- - \text{K}^+$, $\text{Cl}^- - \text{SO}_4^{2-}$, $\text{Mg}^{2+} - \text{Ca}^{2+}$, $\text{Na}^+ - \text{Ca}^{2+}$, Mg^{2+} , SO_4^{2-} , $\text{K}^+ - \text{Ca}^{2+}$ (Tables 3). In general, most ions are positively correlated with Cl^- , especially Na^+ , Mg^{2+} , K^+ , and SO_4^{2-} , indicating that such ions are derived from the same source of saline waters (Kim et al. 2003; Chidambaram et al. 2013), chemical weathering along with leaching of secondary salts (Chidambaram et al. 2009; Prasanna et al. 2010). This trend also indicates the influences of evaporation, agricultural activities, poor drainage conditions, and marine sources (Rao et al. 2012).

In POM, good correlation exhibits between $\text{Cl}^- - \text{Ca}^{2+}$, $\text{Cl}^- - \text{Mg}^{2+}$, $\text{Cl}^- - \text{Na}^+$, $\text{Cl}^- - \text{HCO}_3^-$, $\text{Ca}^{2+} - \text{Mg}^{2+}$, $\text{Na}^+ - \text{Ca}^{2+}$, Mg^{2+} , $\text{SO}_4^{2-} - \text{Ca}^{2+}$, Mg^{2+} , Na^+ , Cl^- (Table 4). Poor correlation is exhibited by HCO_3^- , F^- , NO_3^- , SO_4^{2-} , H_4SiO_4 , and PO_4^- with other ions indicating the effective leaching of these ions due to percolating rainwater to the aquifer matrix (Briz-Kishore and Murali 1992). It is also noted that majority of the ions exhibiting good correlation between Cl^- and SO_4^{2-} with Ca^{2+} , Mg^{2+} , Na^+ , K^+ during both seasons is likely due to the impact of seawater intrusion (Singaraja et al. 2014a), salt

Table 3 Correlation analysis of groundwater samples collected during PRM

	pH	Ca ²⁺	Mg ²⁺	Na ⁺	K ⁺	Cl ⁻	HCO ₃ ⁻	NO ₃ ⁻	PO ₄ ³⁻	F ⁻	SO ₄ ²⁻	H ₄ SiO ₄
pH	1.00											
Ca ²⁺	-0.30	1.00										
Mg ²⁺	-0.28	0.75	1.00									
Na ⁺	-0.31	0.47	0.73	1.00								
K ⁺	-0.34	0.67	0.38	0.32	1.00							
Cl ⁻	-0.33	0.70	0.88	0.94	0.46	1.00						
HCO ₃ ⁻	-0.07	0.12	0.11	0.24	0.16	0.18	1.00					
NO ₃ ⁻	-0.18	0.05	0.17	0.39	0.20	0.32	0.13	1.00				
PO ₄ ³⁻	-0.10	0.00	-0.01	0.02	0.12	0.00	0.04	0.08	1.00			
F ⁻	0.21	-0.14	-0.08	-0.08	-0.10	-0.13	0.41	-0.06	-0.06	1.00		
SO ₄ ²⁻	-0.25	0.37	0.38	0.53	0.18	0.47	0.14	0.33	0.08	0.13	1.00	
H ₄ SiO ₄	-0.05	0.17	0.10	-0.13	0.01	-0.03	-0.12	-0.08	-0.15	0.01	-0.04	1.00

Table 4 Correlation analysis of groundwater samples collected during POM

	pH	Ca ²⁺	Mg ²⁺	Na ⁺	K ⁺	Cl ⁻	HCO ₃ ⁻	NO ₃ ⁻	PO ₄ ³⁻	F ⁻	SO ₄ ²⁻	H ₄ SiO ₄
pH	1.00											
Ca ²⁺	-0.38	1.00										
Mg ²⁺	-0.16	0.72	1.00									
Na ⁺	-0.12	0.69	0.77	1.00								
K ⁺	-0.34	0.27	0.43	0.21	1.00							
Cl ⁻	-0.16	0.75	0.88	0.97	0.28	1.00						
HCO ₃ ⁻	-0.09	-0.02	0.01	0.19	0.04	0.11	1.00					
NO ₃ ⁻	0.07	0.07	0.04	0.05	0.26	0.05	0.04	1.00				
PO ₄ ³⁻	0.00	0.02	-0.04	-0.03	0.12	-0.04	0.00	0.13	1.00			
F ⁻	0.13	-0.11	-0.07	-0.04	-0.11	-0.08	0.35	-0.05	-0.10	1.00		
SO ₄ ²⁻	-0.08	0.65	0.66	0.52	0.23	0.55	-0.04	0.18	-0.03	0.11	1.00	
H ₄ SiO ₄	-0.04	-0.23	-0.40	-0.47	-0.16	-0.48	0.05	-0.22	-0.01	0.15	-0.16	1.00

pan (Smith et al. 2004) in coastal region, and leaching of the secondary salts precipitated along the fissures or the permeable zones of the formations (Chidambaram et al. 2009). The major ions show good, moderate-to-high correlation with other ions and NO_3^- during PRM, which has higher representation of the anthropogenic effluents. The negative relation of pH with Mg^{2+} during all the seasons may be due to the dominance of ion exchange process (Chapelle 1983).

4.7 Factor analysis

In PRM, FA identifies four significant factors explaining 67.78 % of the total data variability (TDV). Factor I comprises Ca^{2+} , Mg^{2+} , Na^+ , Cl^- , NO_3^- , and SO_4^{2-} (Table 5). The association of the ions shows the predominance of seawater intrusion in this aquifer. Panagopoulos et al. (2004) studied the hydrochemical processes in a coastal aquifer and showed that high concentrations of SO_4^{2-} are related to mixing with seawater. Moreover, the association of NO_3^- is an indicative of anthropogenic influence, which may be due to the fact that salt pan area has been increased at the expense of agricultural land, coastal sand with/without vegetation, sand dunes, scrub, and mudflats (Gangai and Ramachandran 2010). This trend is a cause of concern as these pans are fed by both bore wells and sea brine, and this has seriously affected the groundwater table.

Factor 2 was represented by Ca^{2+} , K^+ , and PO_4^- leaching of secondary salts (Chidambaram et al. 2013; Singaraja et al. 2013b) and may be due to the anthropogenic impact from the agricultural practices and mainly due to phosphate fertilizers (Prasanna et al. 2010). Factor 3 represented by F^- and HCO_3^- indicates the weathering process. Similar observations were obtained in the groundwater of Dindigul District of Tamil Nadu (Chidambaram et al. 2013). High-fluoride groundwater is generally associated with high bicarbonate ions and in some cases with high nitrate ions (Tables 5, 6). Factor 4 represented by H_4SiO_4 indicates the weathering of silicate minerals (Thivya et al. 2013b). The study area is predominantly of aluminosilicates, and these undergo weathering to release silica into solution (Chidambaram 2000).

In POM, four factors were extracted with 69.06 % of TDV. Factor 1 was represented by Ca^{2+} , Mg^{2+} , Na^+ , K^+ , and Cl^- , and SO_4^{2-} (Tables 7, 8) resembles the concentration of seawater (Senthilkumar et al. 2008; Prasanna et al. 2010; Chidambaram et al. 2013). Factor 2

Table 5 Factor analysis for the PRM samples (varimax rotated)

	1	2	3	4
pH	-0.26	-0.54	0.17	0.11
Ca^{2+}	0.56	0.61	0.02	0.40
Mg^{2+}	0.80	0.32	-0.01	0.27
Na^+	0.91	0.15	0.02	-0.14
K^+	0.26	0.78	0.08	0.11
Cl^-	0.91	0.31	-0.02	0.06
HCO_3^-	0.15	0.17	0.80	-0.13
NO_3^-	0.48	-0.01	-0.03	-0.50
PO_4^{3-}	-0.21	0.54	0.02	-0.54
F^-	-0.05	-0.22	0.85	0.06
SO_4^{2-}	0.65	0.06	0.17	-0.21
H_4SiO_4	-0.04	0.06	-0.06	0.69

Table 6 Factor representations and total data variability during PRM

Factor	Loadings	TDV (%)
Factor 1	Ca ²⁺ , Mg ²⁺ , Na ⁺ , Cl ⁻ , NO ₃ ⁻ , and SO ₄ ²⁻ , and with negative loading of pH, H ₄ SiO ₄ , and PO ₄ ⁻	35.10
Factor 2	Ca ²⁺ , K ⁺ , and PO ₄ ⁻ with negative loading of pH, NO ₃ ⁻ , F ⁻	12.85
Factor 3	HCO ₃ ⁻ and F ⁻ with negative loading of Mg ²⁺ , Cl ⁻ , NO ₃ ⁻ , and H ₄ SiO ₄	10.83
Factor 4	H ₄ SiO ₄ with negative loading of Na ⁺ , HCO ₃ ⁻ , NO ₃ ⁻ , and SO ₄ ²⁻	9.01

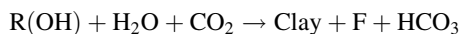
Table 7 Factor analysis for the POM samples (varimax rotated)

	1	2	3	4
pH	-0.13	0.04	-0.87	0.01
Ca ²⁺	0.81	-0.08	0.33	-0.02
Mg ²⁺	0.91	-0.05	0.13	0.03
Na ⁺	0.92	0.08	-0.02	-0.02
K ⁺	0.29	-0.02	0.51	0.54
Cl ⁻	0.96	0.00	0.03	0.00
HCO ₃ ⁻	0.06	0.81	0.11	0.08
NO ₃ ⁻	0.09	0.07	-0.19	0.80
PO ₄ ³⁻	-0.10	-0.07	0.11	0.56
F ⁻	-0.04	0.81	-0.15	-0.13
SO ₄ ²⁻	0.71	0.10	0.06	0.05
H ₄ SiO ₄	-0.53	0.22	0.37	-0.30

Table 8 Factor representations and total data variability during POM

Factor	Loadings	TDV (%)
Factor 1	Ca ²⁺ , Mg ²⁺ , Na ⁺ , Cl ⁻ , and SO ₄ ²⁻ with negative loading of pH, PO ₄ ⁻ , F ⁻ , and H ₄ SiO ₄	35.89
Factor 2	HCO ₃ ⁻ and F ⁻ with negative loading of Ca ²⁺ , Mg ²⁺ , K ⁺ , and PO ₄ ⁻	12.16
Factor 3	K ⁺ and with negative loading of pH, Na ⁺ , NO ₃ ⁻ , and F ⁻	10.64
Factor 4	K ⁺ , NO ₃ ⁻ , and PO ₄ ⁻ with negative loading of Ca ²⁺ , Na ⁺ , F ⁻ , and H ₄ SiO ₄	10.36

samples are represented mainly by F⁻ and HCO₃⁻, which shows the weathering and release of F⁻ from hydroxyl group of mineral, which is confirmed by very low representation of pH.



R indicates the silicate mineral. It is also fascinating point to note that low concentration of Ca²⁺ and Mg²⁺ corresponding to high fluoride in the water has earlier been reported by Nanyaro et al. (1984) and Teotia et al. (1981). Factors III and IV represented by K⁺, NO₃⁻, and PO₄⁻ indicate the anthropogenic impact due to the agricultural practices and mainly due to phosphate and potash fertilizers (Prasanna et al. 2010). It is also interesting to note that during PRM, Factor 3 is represented by F⁻ and HCO₃⁻, which subsequently during POM gains momentum as Factor 2 which is again represented by F⁻ and HCO₃⁻. This incidence represents the enhancement of F⁻ factor from PRM (Factor 3) to POM (Factor 2)

due to the dominance of weathering process and release of F^- from hydroxyl group of mineral, which is confirmed by very low representation of pH during POM session (Chidambaram et al. 2013).

4.8 Factor scores

Factor score is used to reveal the spatial variation in chemical processes. Factor scores were calculated for each sample. Dalton and Upchurch (1978) have shown that factor scores for each sample can be related to the intensity of the chemical process described by the factor. The factor score was also estimated to find out the spatial variation in the factor representation and to identify the positive zone of its representation. Figure 7a shows the spatial distribution of factor scores for first factor during PRM period, indicating the probability zones of the saltwater intrusion. The values >0.1 fall in the eastern part of the study area along the coast, covering an area of about 409.3 km^2 followed by the region covered by values ranging from -0.26 to 0.1 falling in the eastern part of the study area, covering an area of about 781.6 km^2 .

The spatial distribution of the factor score during POM (Fig. 7b) shows that the intensity of saltwater activity is well noted along the coastal area ranges from >0.01 falling in the eastern part of the study area along the coast and salt pan, covering a region of about 404.3 km^2 followed by the values -0.26 to 0.01 , total area covering about 1071 km^2 . Seawater intrusion is higher in the PRM period as compared to the POM period. It may be also due to higher amount of groundwater exploration in this area due to dry climate condition exists in this area during this period. It is also noted that higher scores are located in the northeastern part of study area along the coastal region. Further, high concentration of Cl^- in water may be attributed to contamination by anthropogenic sources such as industrial discharge (Rasouli and Masoudi 2012). Another source of high Cl^- in shallow groundwater is the evaporation of surface water and moisture in the unsaturated zone (Richter and Kreitler 1993). The spatial distributions of the factor score show that the

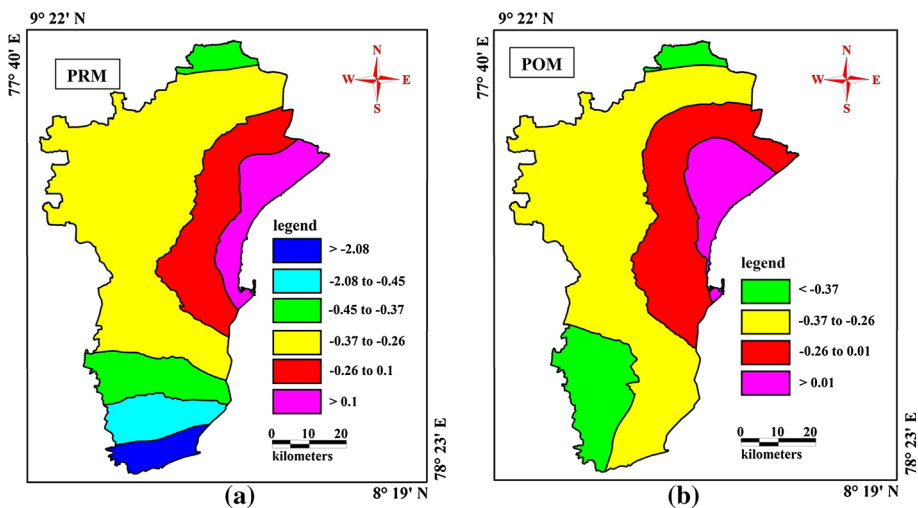


Fig. 7 a Spatial distribution of Factor 1 during PRM in groundwater. b Spatial distribution of Factor 1 during POM in groundwater

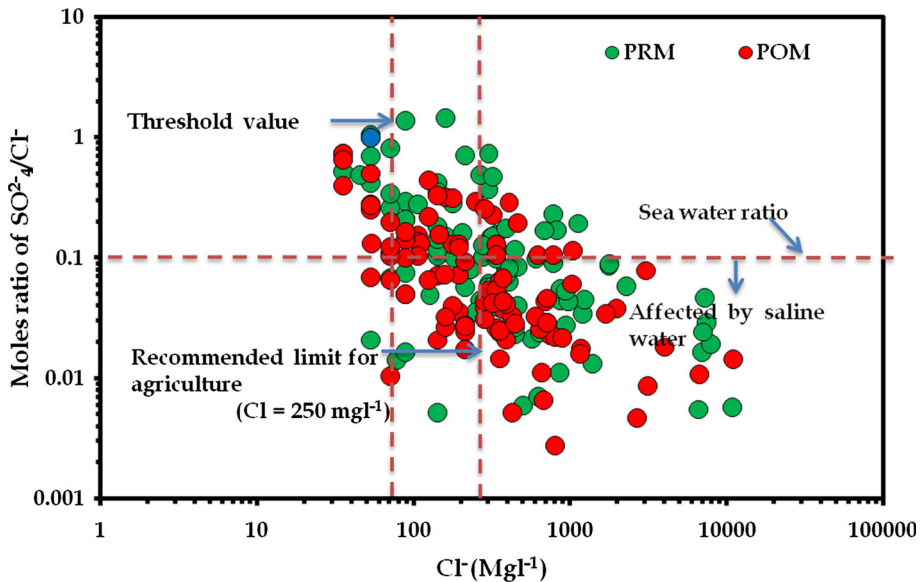


Fig. 8 Molar ratios of $\text{SO}_4^{2-}/\text{Cl}^-$ versus Cl^- concentration during PRM and POM seasons

intensity of saltwater and salt pan activity is well noted along the coastal area, eastern part of the study area. It is clearly evident that the $\text{SO}_4^{2-}/\text{Cl}^-$ ratio (Fig. 8) in this region shows that there are regions with low SO_4^{2-} and high SO_4^{2-} compared to the standard seawater. Chivas et al. (1991) proved that the oxidation of organic diethyl sulfide gas (DMS) released from productive upwelling coastal waters is an important source of SO_4^{2-} inland. The enrichment in SO_4^{2-} compared to Cl^- in the pan waters may reflect similar input of DMS, which enriches the SO_4^{2-} in groundwater resulting in high $\text{SO}_4^{2-}/\text{Cl}^-$ ratios. Sulfate-to- Cl^- ratios influenced by salt pan water show increasingly scattered at high salinities with a number of water samples plotting below the predicted conservative $\text{SO}_4^{2-}/\text{Cl}^-$ line (Smith et al. 2004). It is interesting to note that higher concentration prevails during both seasons.

4.9 Stability of water

[Na]/H, [K]/H, [Ca]/H, and [Mg]/H ratios for groundwater from study area were plotted on the stability diagram (Figs. 9, 10, 11, 12) as a function of [H₄SiO₄].

4.9.1 Na-silicate system

The PRM samples (Fig. 9) fall in the Na-montmorillonite stability field, and along this Kaolinite boundary, they move toward the kaolinite field during the POM. The movement of stability from the kaolinite to montmorillonite is expected due to the supply of excess cation to the preexisting kaolinite, which also appears to be formed owing to evaporation processes as suggested by Jacks (1973). Majority of the POM samples fall in the kaolinite field, and they move toward Na-montmorillonite field in PRM; it is to be observed that the silica concentration has decreased in the post-monsoon samples. This may be due to the leached effect after the monsoon or increase in silicate weathering. It is understood that the

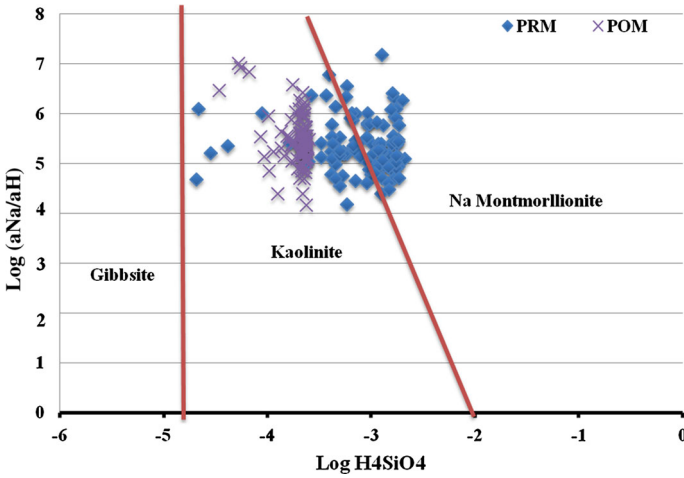


Fig. 9 Thermodynamic stability of Na system for samples representing different seasons

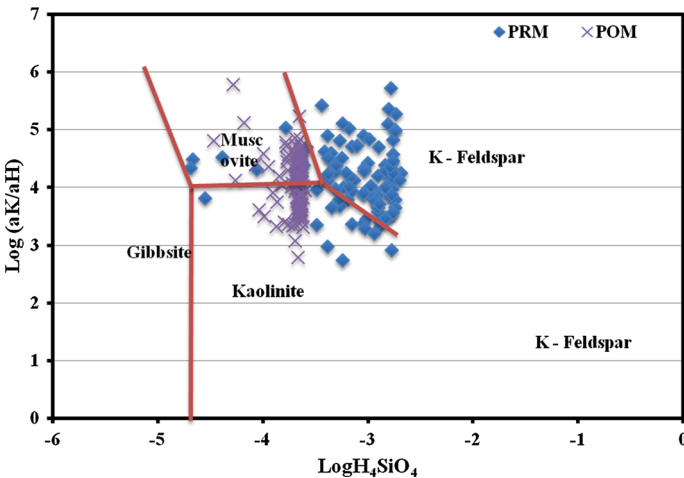


Fig. 10 Thermodynamic stability of K system for samples representing different seasons

Na cation is more mobile than the silica during the monsoon season, and hence, there is a vertical shift in the stability field. Silica concentration increases during PRM, and the sample representations of these seasons are also noted in the Na-montmorillonite field with few scattered representations in the kaolinite field. The sources of Na in the system may be due to weathering of plagioclase weathering, ion exchange, or due to seawater intrusion.

4.9.2 K-silicate system

Majority of POM (Fig. 10) samples fall in kaolinite field, and muscovite then distributes the samples during PRM fall in the muscovite and kaolinite fields. The diagram delineates the stability field of clay minerals that coexist in matrix phase at a constant composition of

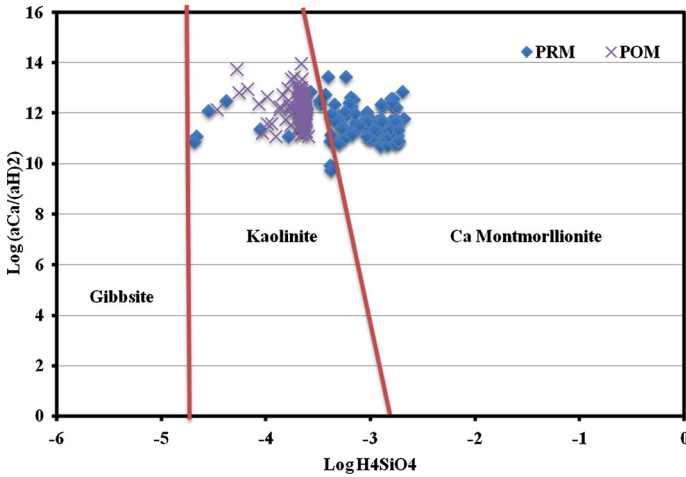


Fig. 11 Thermodynamic stability of Ca system for samples representing different seasons

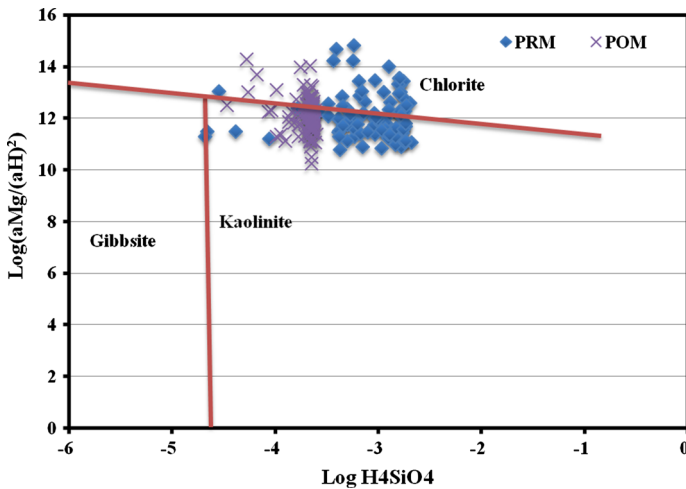


Fig. 12 Thermodynamic stability of Mg system for samples representing different seasons

water during chemical reaction of rock and water. It is evident that movement of chemical composition from muscovite to kaolinite released silica. Hence, H_4SiO_4 has increased in groundwater (Chidambaram et al. 2007) during the process of migration of the composition toward K-feldspar. It can be understood from this that there are two different pathways of thermodynamic stability migration

Pathway 1: Gibbsite kaolinite K-feldspar

Pathway 2: Gibbsite muscovite K-feldspar

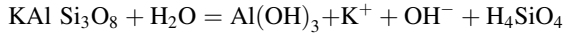
The entire hydrogeochemical process represents the dissolution of minerals; the K system represents two different pathways:

Pathway 1

The first pathway shows migration of the aqueous compositional stability from gibbsite to kaolinite and then to K-feldspar

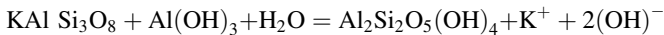
a. K-feldspar to gibbsite

Feldspars break down to gibbsite ($\text{Al}(\text{OH})_3$) setting silica free as dissolved silicic acid, and then, kaolinite is formed by later reaction between $\text{Al}(\text{OH})_3$ and H_4SiO_4 :



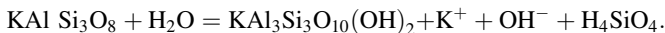
b. Gibbsite to kaolinite

The second reaction involves minor amount of Al that goes into solution in which Al and Si are both separated from feldspars as colloidal particle which later joins to form kaolinite (Krauskopf 1979)

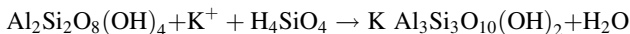


c. Kaolinite to K-feldspar

Feldspars in rocks would react with water and release H_4SiO_4 . That H_4SiO_4 released is consumed for the conversion of gibbsite to kaolinite. The solution composition moves to gibbsite–kaolinite boundary unit, and all gibbsite have been used up. Here, from gibbsite, stability field would move to kaolinite. Then, solution boundary moves from kaolinite to muscovite boundary until all kaolinite are used up.



Shift of stability from kaolinite to muscovite is the addition of K^+ and SiO_2 to kaolinite. The probable equation is:



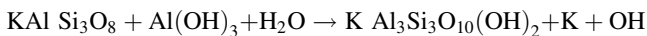
Pathway 2

The second pathway shows migration of the aqueous compositional stability from gibbsite to muscovite and then to K-feldspar

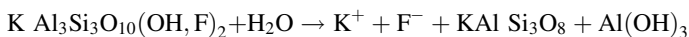
K-feldspar to gibbsite



Gibbsite to muscovite



Muscovite to K-feldspar



The main process that governs the migration of the compositional pathways is the availability of K^+ ions. It is noticed that the first pathway is more significant in all the seasons. Minor representations of POM samples show representations of the pathway 2. The PRM samples are dominantly stable with the K-feldspar field. This is due to the

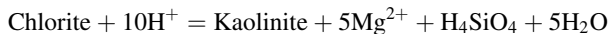
mobility of K^+ during the monsoon than the other seasons; this may be due to the migration of ions during weathering, ion exchange, or other anthropogenic impacts.

4.9.3 Ca–silicate system

The plot exhibits the migration from kaolinite to Ca-montmorillonite field in most of the samples during PRM season. The samples of PRM fall in Ca-montmorillonite field, which may be due to the higher concentration of Ca. But during POM (Fig. 11), most of the samples fall in kaolinite field due to the decrease in silica in the groundwater.

4.9.4 Mg–silicate system

In POM seasons (Fig. 12), the samples are stable with kaolinite field, and few samples of PRM exhibit high Mg and H_4SiO_4 . Hence, these samples fall in chlorite stability field. During PRM, few samples are shifted from kaolinite field to chlorite field due to the increase in the concentration of Mg^{2+} . Seasonal variations indicate that the shift of samples between two fields, i.e., kaolinite and chlorite, is due to the forward or reverse nature of reaction (Chidambaram et al. 2007). The samples irrespective of seasons are stable with kaolinite field, and few represented samples of PRM exhibit high Mg (Fig. 12). Hence, these samples fall in chlorite stability field.



The majority of samples of all the seasons fall in kaolinite field as the concentration of Mg^{2+} is insufficient to form the chlorite stability. Seasonal variations indicate the shift of samples between two fields, i.e., kaolinite and chlorite, due to the forward or reverse nature of reaction (Chidambaram et al. 2007).

5 Water classification

5.1 Water quality for drinking purposes

The quality of groundwater is important because it determines the suitability of water used for drinking, domestic, and irrigation purposes (Yidana et al. 2010; Oinam et al. 2012; Singaraja et al. 2013a). Water quality index (WQI) is an essential parameter for demarcating groundwater quality and its suitability for drinking purposes (Singh 1992; Rao 1997; Mishra and Patel 2001; Avvannavar and Shrihari 2008). WQI is defined as a technique of rating that provides the composite influence of individual water quality parameters on the overall quality of water (Mitra and ASABE Member 1998) for human consumption. The standards for drinking water quality purposes as recommended by WHO (2004) have been considered for the calculation of WQI. For computing WQI, four steps are followed.

First step

Each of the 11 parameters (pH, TDS, Cl^- , HCO_3^- , SO_4^{2-} , NO_3^- , F^- , Ca^{2+} , Mg^{2+} , Na^{2+} , and K^+) has been assigned a weight (w_i) according to its relative substance in the overall quality of water for drinking purposes (Table 9). The maximum weight of 5 has been assigned to the parameters such as total dissolved solids, chloride, fluoride, and sulfate due to their major importance in water quality assessment (Srinivasamoorthy et al. 2008). Bicarbonate and potassium are given the minimum weight of 2 as it plays an

Table 9 Relative weight of chemical parameters

Parameters	WHO standard	Weight (w_i)	Relative weight (W_i)
pH	6.5	3	0.073
TDS (mg l^{-1})	500	5	0.122
Ca^{2+} (mg l^{-1})	100	3	0.073
Mg^{2+} (mg l^{-1})	50	4	0.098
Na^+ (mg l^{-1})	200	4	0.098
K^+ (mg l^{-1})	20	2	0.049
HCO_3^- (mg l^{-1})	125	1	0.024
Cl^- (mg l^{-1})	250	5	0.122
SO_4^{2-} (mg l^{-1})	200	5	0.122
NO_3^- (mg l^{-1})	45	4	0.098
F^- (mg l^{-1})	1.5	5	0.122
		Total of weight = 41	Total of relative weight = 1

insignificant role in the water quality assessment. Other parameters such as calcium, magnesium, sodium, pH, and nitrate were assigned weight between 1 and 5 depending on their importance in water quality determination.

Second step

The relative weight (W_i) is computed from the following equation:

$$W_i = w_i / \sum_{i=1}^n w_i$$

where W_i is the relative weight, w_i is the weight of each parameter, n is the number of parameters.

Calculated relative weight (W_i) values of each parameter are given in Table 9.

Third step

A quality rating scale (q_i) for each parameter is assigned by dividing its concentration in each water sample by its relevant standard according to the guidelines laid down in the WHO (2004), and the result is multiplied by 100:

$$q_i = (C_i/S_i) \times 100$$

where q_i is the quality rating, C_i is the concentration of each chemical parameter in each water sample in milligrams per liter, S_i is the world drinking water standard for each chemical parameter in milligrams per liter according to the guidelines of the WHO (2004).

Fourth step

For computing the WQI, the SI is first determined for each chemical parameter, which is then used to determine the WQI as per the following equation

$$\text{SI}_i = W_i \times q_i$$

$$\text{WQI} = \sum \text{SI}_i$$

where SI_i is the subindex of i th parameter, q_i is the rating based on the concentration of i th parameter.

Table 10 WQI range, type of water, and percentage of the water samples during PRM and POM

Range	Type of water	Percentage of the samples	
		PRM	POM
<50	Excellent water	19	28
50–100.1	Good water	31	39
100–200.1	Poor water	29	20
200–300.1	Very poor water	12	6
>300	Water unsuitable for drinking purposes	9	7

Water quality types were determined on the basis of WQI. The computed WQI values range from 23.67 to 1373.81 and 30.02 to 934.45 for PRM and POM, respectively. The WQI range, type of water, and calculation of WQI for percentage samples can be classified in Table 10. During PRM, 19 % of groundwater samples represent “excellent water,” 31 % indicate “good water,” 29 % show “poor water,” 12 % show “very poor water,” and 9 % indicate unsuitable for drinking purposes. During POM, 28 % sample signify “excellent water,” 39 % show “good water,” 20 % show “poor water,” 6 % of sample show “very poor water,” and remaining 7 % of the samples fall on unsuitable for drinking purposes. The PRM samples show signs of poor quality in drinking purpose compared to POM. This may be due to dilution of ions after monsoon, over exploitation of groundwater, direct discharge of effluents, and agricultural impact (Singaraja et al. 2013b; Thivya et al. 2013a; Thilagavathi et al. 2014; Singaraja et al. 2014b).

Spatial distribution of WQI shows four zones such as excellent, good, poor to very poor, and unsuitable water for drinking purpose during both seasons. Zone 1, eastern part of the study area along the coast, covers a region of about 265.6 and 50.30 km² during PRM and POM unsuitable for drinking purpose. Zone 2 covers an area of 689.05 and 368.1 km² during PRM and POM, it is parallel to the coast and bounds Zone 1 in the

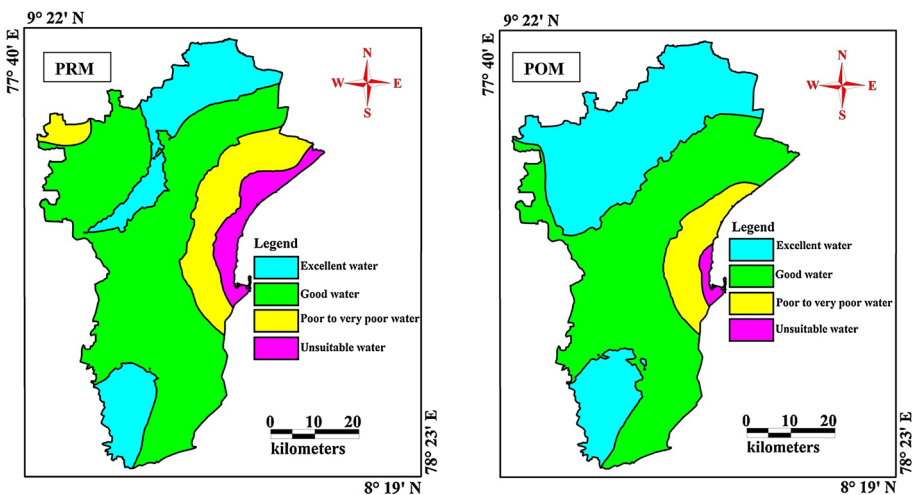
**Fig. 13** Spatial distribution of WQI during both seasons

Table 11 Formula applied for the calculation for various parameters (all values in meq l⁻¹)

Equation	Parameters	References
Na %	$(\text{Na}^+ + \text{K}^+)/(\text{Ca}^{2+} + \text{Mg}^{2+} + \text{Na}^+ + \text{K}^+) \times 100$	Wilcox (1955)
SAR	$\text{Na}^+/\sqrt{\text{Ca}^{2+} + \text{Mg}^{2+}}/2$	Richard (1954)
RSC	$(\text{CO}_3 + \text{HCO}_3^-) - (\text{Ca}^{2+} + \text{Mg}^{2+})$	Richard (1954)
RSBC	$\text{HCO}_3^- - \text{Ca}^{2+}$	Gupta and Gupta (1987)
PI	$\{(\text{Na}^+ + \sqrt{\text{HCO}_3^-})/[(\text{Ca}^{2+} + \text{Mg}^{2+} + \text{Na}^+)]\} \times 100$	Doneen (1948)
MH	$[\text{Mg}^{2+}/(\text{Ca}^{2+} + \text{Mg}^{2+})] \times 100$	Raghunath (1987)
PS	$\text{Cl}^- + 1/2\text{SO}_4^{2-}$	Doneen (1954)
KR	$\text{Na}^+/(\text{Ca}^{2+} + \text{Mg}^{2+})$	Kelly's (1963)
TH	$2.497\text{Ca}^{2+} + 4.115 \text{Mg}^{2+}$	Todd (1980)
CR	$\{(\text{Cl}^-/35.5) + (\text{SO}_4^{2-}/96)\}/2(\text{HCO}_3^-) \times 100$	Ryzner (1984)

eastern part of the study area poor to very poor water. Zone 3 cover an area 2691.39 and 2307.39 km² during PRM and POM followed by Zone 2 and it is the central part of the study area in both seasons. Zone 4 falls in the northern and southwestern part of the study area, covering an area of about of 944.5 and 1863.1 km² during PRM and POM (Fig. 13).

6 Irrigation quality

6.1 Sodium percentage

In all natural waters, sodium percentage is the most important parameter in determining the suitability of water for irrigation use (Wilcox 1955) and can be determined using the equation in Table 11, where all the ions are expressed in meq l⁻¹. Na % in the groundwater ranges from 20.39 to 88.67 in PRM and 4.14 to 79.14 in POM season (Table 12). According to Wilcox (1955), 25 and 52 % of the samples fall under good class during PRM and POM, 33 and 19 % fall in permissible class during PRM and POM, 32 and 4 % in doubtful class during PRM and POM, and 10 % in unsuitable class during PRM for irrigation.

Spatial distribution of Na % shows that 25 and 15 % unsuitable for irrigation purpose during PRM and POM season respectively, (Fig. 14) observed in eastern part of the study area along the coastal region as based on Wilcox (1955). It is also noted that eastern part of the study area higher in sodium percentage along the coastal region may be due to seawater intrusion (Nurmi et al. 1988; Singaraja et al. 2013b). High percentages of Na⁺ in the groundwater can feat the plant growth, deflocculating and reducing soil permeability (Singh et al. 2008; Joshi et al. 2009).

6.2 Sodium absorption ratio (SAR)

SAR is an essential parameter for determining the suitability and unsuitability of groundwater for irrigation because it is a measure of alkali/sodium hazard to crops. SAR is calculated by formula in Table 11 (where the concentrations of all ions are in meq l⁻¹). The calculated value of SAR in this area ranges from 0.56 to 48.46 with average 7.16 and

Table 12 Maximum, minimum, and average of the different geochemical quality parameters groundwater representing during both seasons

	Na %	SAR	RSC	PI	KR	MH	RSBC	PS	TH	PSI	CR
PRM											
Avg	55.51	6.68	-8.85	66.92	1.62	53.29	-2.38	26.79	574.35	-30.36	15.54
Min	20.56	0.57	-132.63	24.60	0.25	14.16	-76.24	1.26	49.58	-371.44	0.40
Max	88.77	48.70	3.85	114.56	7.63	89.90	7.40	305.90	6731.70	105.31	215.30
POM											
Avg	58.30	6.79	-2.62	76.21	1.96	45.50	1.49	18.34	408.92	-28.30	6.02
Min	13.39	0.41	-71.18	32.52	0.13	3.54	-26.74	1.20	39.71	-79.18	0.26
Max	92.82	53.41	35.99	124.45	12.78	92.23	43.15	312.25	3738.79	124.68	121.96

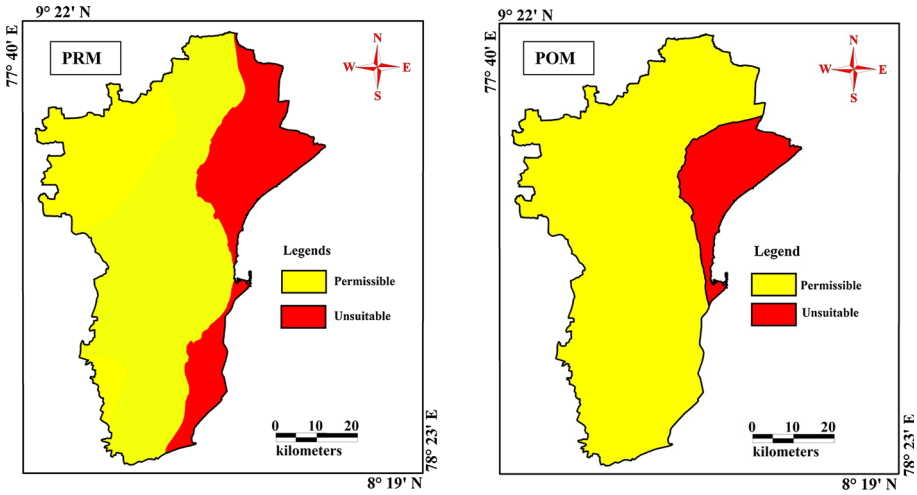


Fig. 14 Spatial distribution of sodium percentage during PRM and POM seasons

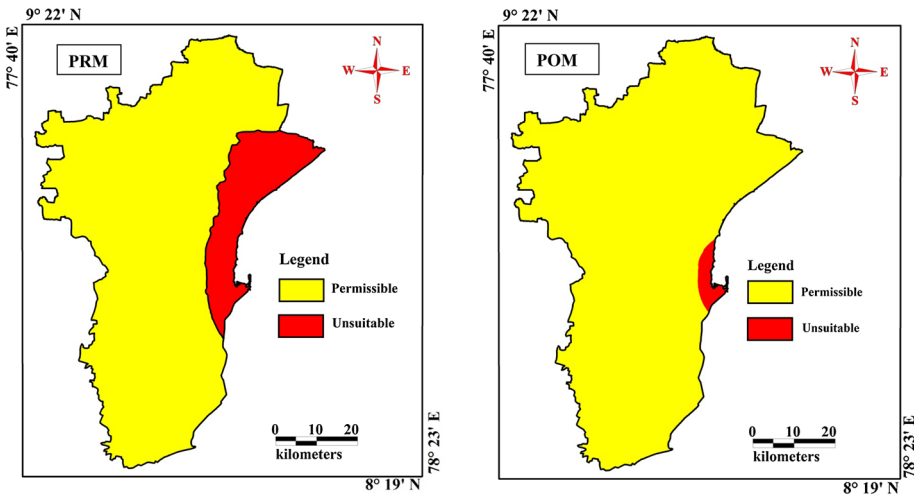


Fig. 15 Spatial distribution of sodium absorption ratio during PRM and POM seasons

0.10 to 56.89 with average 3.88 during PRM and POM seasons, respectively (Table 12). When SAR values are >5–9, irrigation water will cause permeability problems of shrinking and swelling in clayey soils (Saleh et al. 1999).

According to Richard (1954) classification, more than 84 and 93 % of samples fall under excellent class, 6 and 4 % fall under good category, 4 and 1 % of the samples fall under fair category, and remaining 6 and 2 % of the samples fall under poor category during PRM and POM.

Spatial distribution of SAR (Fig. 15) shows that 17 and 5 % of the study area are unsuitable for irrigation purpose along the coastal region during PRM and POM seasons. The higher the SAR values in the water, the greater the risk of Na⁺, which leads to the

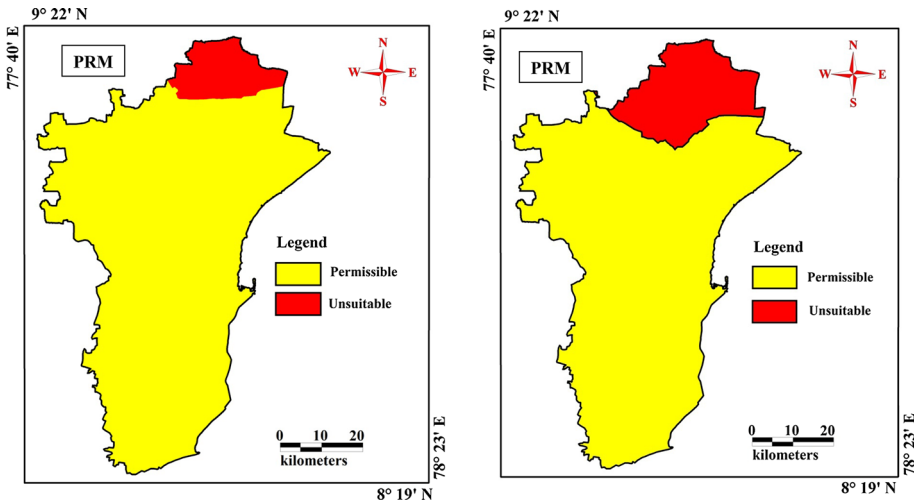


Fig. 16 Spatial distribution of residual sodium carbonate during PRM and POM seasons

development of an alkaline soil (Todd 1980), while a high salt concentration in water leads to the formation of saline soil.

6.3 Residual sodium carbonate (RSC)

The RSC is an index, which indicates the sodium hazards (solidification of soil). The unfit water samples (containing excess of carbonate and bicarbonate) will precipitate soil solution of calcium and increase solution of sodium which, resulting in soil dispersion (Emerson and Bakker 1973) as well as impaired nutrient uptake by plants (Kanwar and Chaudhry 1968). This is defined as RSC (Richards 1954). High concentration of sodium in irrigation water can result in the degradation of soil structure. This will reduce water infiltration into the soil surface, down the profile, and limit aeration, which leads to reduced crop growth.

RSC is calculated by formula in Table 11 (where the concentrations of all ions are in meq l^{-1}). The study area RSC values range from -132.00 to 35 (Table 12). According to Richard's classification, water with RSC >2.5 is considered unsuitable for irrigation. The water with RSC of 1.25 – 2.5 is considered as marginal, and those with a value <1.25 are safe for irrigation purpose. 74 to 95 % of the samples fall in good category during all the seasons. 3 % of samples fall in medium category during PRM and NEM, respectively. It is to be noted that 12 and 16 % of samples during NEM and POM are represented in the bad category and 4 and 2 % of samples during PRM and SWM seasons are represented in the bad category, respectively. Spatial distribution of RSC (Fig. 16) shows that 10 and 15 % of the study area are unsuitable for irrigation purpose during PRM and POM along northern.

6.4 Magnesium hazard (MH)

Szabolcs and Darab (1964) have proposed a MH for assessing the suitability of water quality for irrigation. Generally, Ca^{2+} and Mg^{2+} maintain a state of equilibrium in water, and they do not behave equally in the soil system. Magnesium damages soil structure,

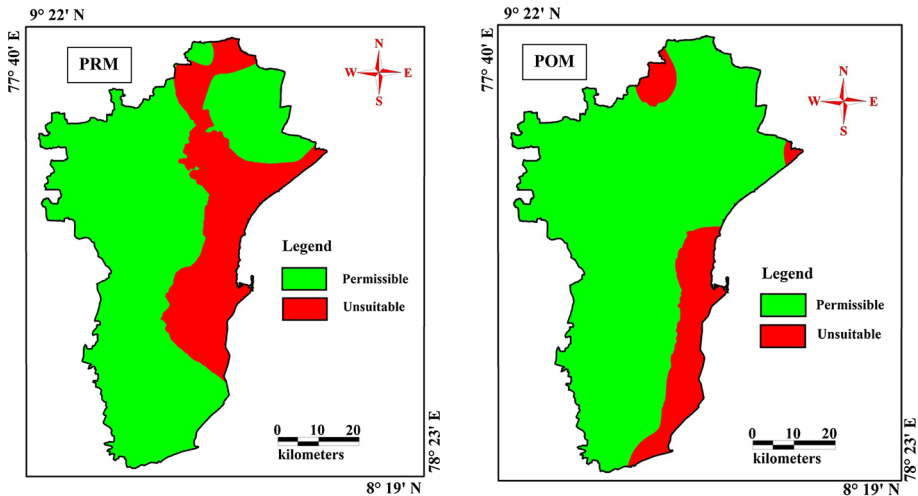


Fig. 17 Spatial distribution of magnesium hazard during PRM and POM

when water contains more Na^+ and high saline. Normally, a high level of Mg^{2+} is caused by exchangeable Na^+ in irrigated soils. In equilibrium, more Mg^{2+} can affect soil quality by rendering alkaline, and hence, it affects crop yields.

Magnesium content in water is considered as one of the most important qualitative criteria in determining the quality of water for irrigation. Generally, in most waters, calcium and magnesium maintain a state of equilibrium. A ratio namely index of MH was developed by Paliwal (1972) and is given in Table 11. According to this, high MH value ($>50\%$) has an adverse affect on the crop yield as the soil becomes more alkaline. MH values of the study area, ranges between from 9.09 to 84.38 during PRM and 14.75 to 84.50 during POM (Table 12). In the study area, 31 and 26 % of the samples were found to be unsuitable for irrigation when $\text{MH} > 50\%$ during PRM and POM. Spatial distribution of MH (Fig. 17) shows that 29 and 19 % of the study area are unsuitable for irrigation purpose during PRM and POM along the coastal region. It is also noted that higher contamination during PRM compared to POM is due to the effect of dilution after monsoon.

6.5 Kelly's ratio (KR)

Kelly's ratio is used to find out the suitability or unsuitability of groundwater for irrigation purpose. Sodium measured against calcium and magnesium was considered by Kelly (1963) for calculating KR equation and is given in Table 11. Groundwater having KR more than one is generally considered unfit for irrigation purposes. KR ranges between 0.39 and 11.92 during PRM and between 0.04 and 14.26 in the POM (Table 12) samples of the study area.

Thirty-one and 78 % of the samples fall on the permissible value of 1 showing a good balance of sodium, calcium, and magnesium ions during PRM and POM season, respectively. But 69 and 22 % of the samples fall on not suitable (>1) for irrigation in the study area during PRM and POM due to poor balance of sodium, calcium, and magnesium ions (Ayers and Wascot 1985). In spatial distribution higher values (>1) of KR observed in the eastern part of the study area during both season respectively (Fig. 18). 57 and 3 % of the

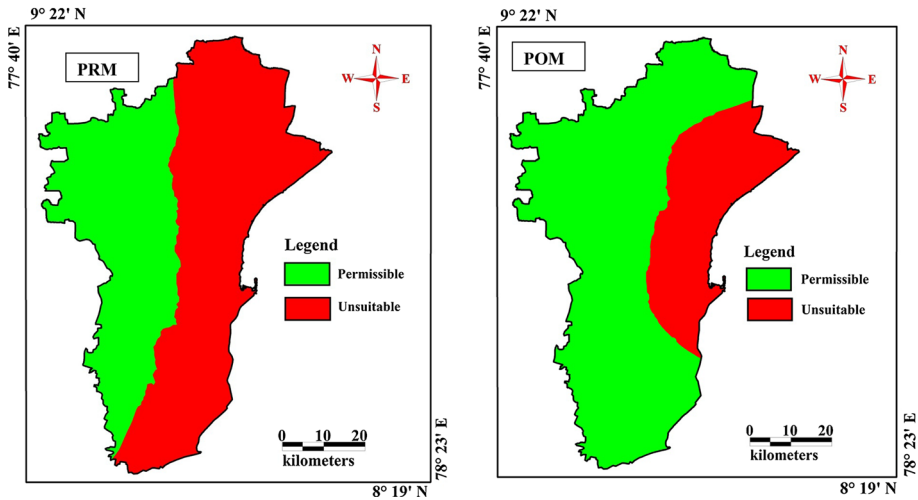


Fig. 18 Spatial distribution of Kelly's ratio during PRM and POM seasons

region out of total region are unfit for irrigation purpose during PRM and POM. It is also noted that higher contamination in PRM compared to POM is due to the influence of dilution effect after monsoon.

6.6 Puri's Salt Index

Puri (1949) established an index to interpret the quality of irrigation water. The PSI was calculated by equation in Table 8. The PSI ranges vary from -24.5 to 0 for good-quality waters and 0 to $+ve$ (positive) values for poor-quality waters. The study area values varied from -6858.50 to 3087.53 during PRM and -1438.2 to 3682.3 during POM (Table 12).

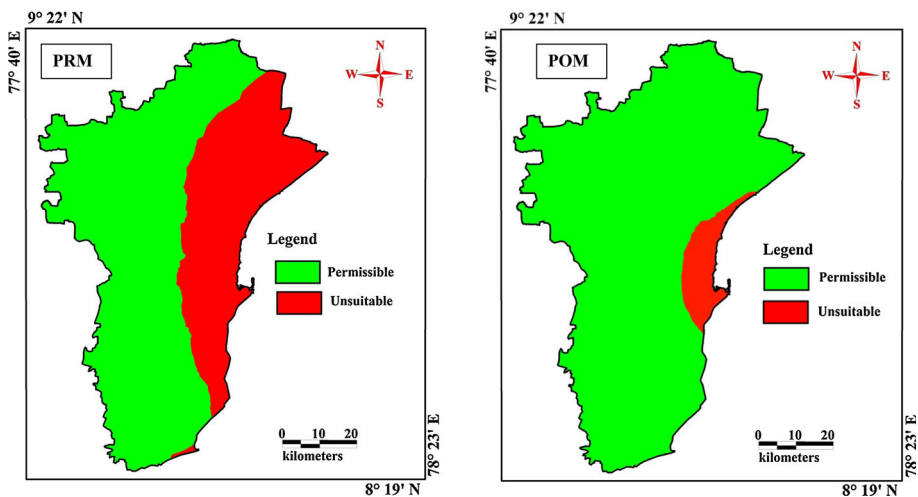


Fig. 19 Spatial distribution of Puri's Salt Index during PRM and POM seasons

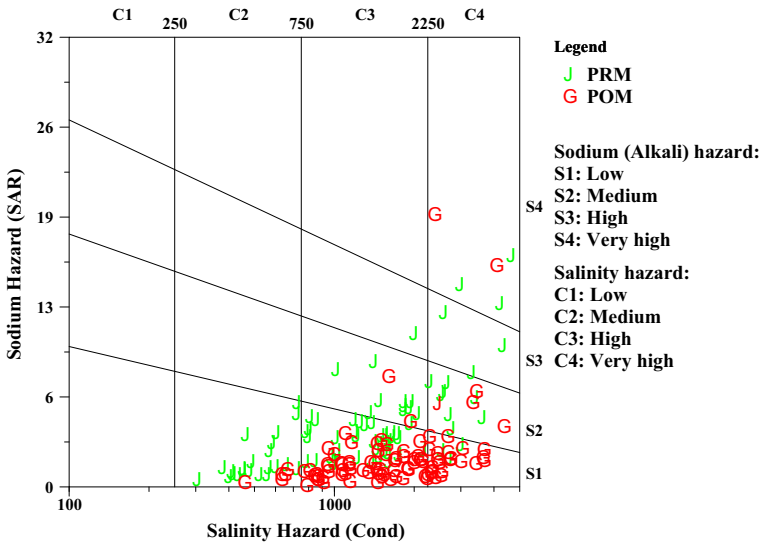


Fig. 20 USSL classification of irrigation groundwater during pre- and post-monsoon (based on Richards 1954)

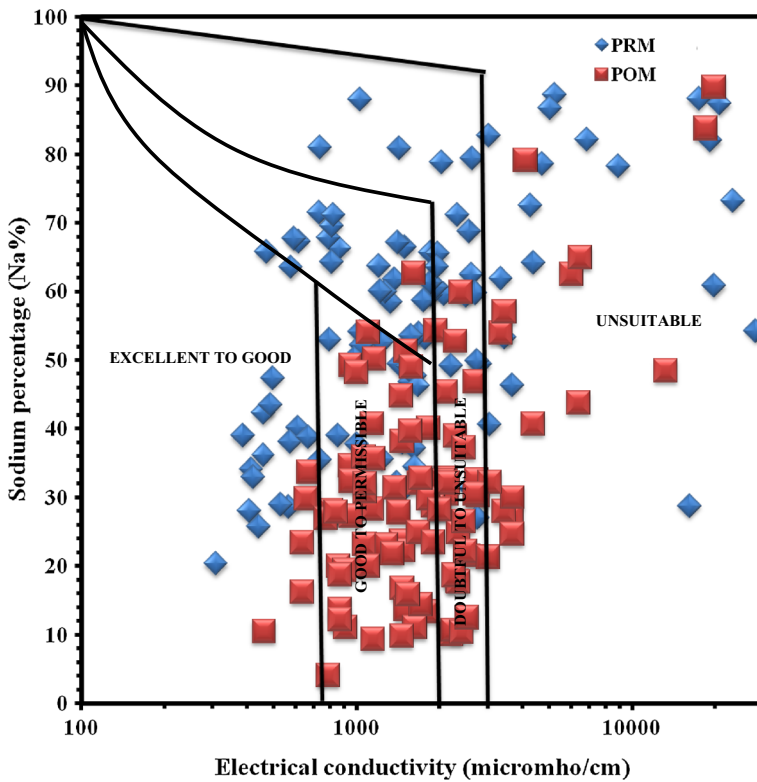


Fig. 21 Plot of sodium percentage and electrical conductivity (based on Wilcox 1955) for the classification of groundwater for irrigation uses during PRM and POM

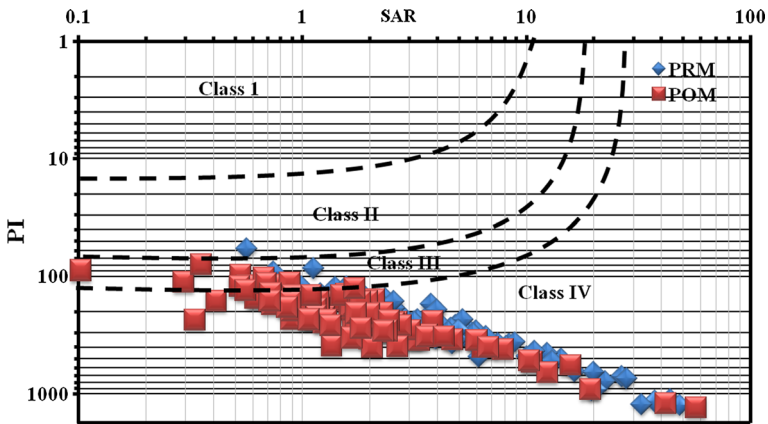


Fig. 22 Modified Doneens plot for the identification of the irrigation suitability of water for PRM and POM

73 and 92 % of the samples showed negative values during PRM and POM, and 27 and 8 % of the sample fall on poor-quality water for irrigation purpose due to positive values, indicating free Na^+ ions in the irrigation water during PRM and POM. Free Na^+ ions are prevalent in many samples. Continuous irrigation with the groundwater having excess free Na^+ will lead to Na^+ accumulation in soils.

Spatial distribution of PSI (Fig. 19), 0 to +ve (positive) values was observed in both seasons in the eastern part due to the coastal area. 30 and 6 % of the area are unsuitable for irrigation purpose during PRM and POM seasons, respectively. It is also noted that major part of the unsuitable for irrigation purpose during PRM compared to POM is due to the dilution effect after monsoon.

In order to classify the groundwater samples for irrigation uses, three diagrams, i.e., the US salinity diagram (1954), Wilcox classification diagram (1955), and Doneen modified diagram, have been used (see Figs. 20, 21, 22).

6.7 US Salinity Laboratory's diagram (USSL)

The USSL (1954) diagram best explains the combined effect of sodium hazard and salinity hazard. The US Salinity Laboratory's diagram (Fig. 20) is used widely for rating irrigation water where SAR is plotted against EC (Richards 1954). The plot of data on the US salinity diagram shows that the water samples were found mostly confined in four classes of water type, i.e., C2-S1, C3-S1, C3-S2, C3-S3, C4-S1, C4-S2, C4-S3, and C4-S4. Some water samples fall beyond the limits of the diagram. Low sodium and medium salinity water of C2-S1 class can be used for irrigation, if a moderate amount of leaching occurs (Khodapanah et al. 2009). Water of C4-S4 class generally is not suitable for irrigation. Salinity in C3-S2, C4-S3, and C4-S4 classes is high and very high. It produces sodium problem in most soils and not suitable for irrigation. This figure found that most of the samples were unsuitable.

6.8 Wilcox diagram

Analytical data were plotted on the Wilcox diagram (1955) relating EC and sodium percentages. According to Wilcox diagram (Fig. 21), the study area's groundwater samples fall almost in all classes of the diagram. Most of the PRM groundwater samples fall on

good to permissible quality and may be used for irrigation purposes, and few PRM samples fall on excellent to good category. This diagram clearly indicates that most of the PRM groundwater samples are unsuitable for irrigation purpose compared to POM due to the dilution effect after monsoon.

6.9 Water infiltration rate (Doneen)

Based on the permeability index and SAR, a new plot has been designed, and samples were fall in Class II, Class III, and Class IV (Fig. 22). The majority of the samples in both the seasons are represented in Class III and Class IV during PRM and POM, but only one sample is represented in Class II during PRM. It is worth noting that most of the groundwater samples fall on (Class IV) unsuitable for irrigation purpose during PRM compared to POM due to the influence of dilution effect after monsoon.

7 Classification for domestic purpose

Hardness refers to the reaction with soap and formation of scale. It increases the boiling point but does not have adverse effect on human health. In the study area, 50 and 43 % of the samples fall in the very hard category during PRM and POM. Spatial distribution of TH (Fig. 23) shows that 17 and 12 % of the area are covered by very hard categories and 38 and 21 % of the study area are covered by moderately hard categories.

$$TH = 2.497Ca^{2+} + 4.115Mg^{2+}$$

Chloro-alkaline indices, i.e., CAI1 and CAI2, are used to measure the extent of base exchange during rock–water interaction, where there is an exchange of Na^+ and K^+ in groundwater with Mg^{2+} or Ca^{2+} in rock matrix when both the indices are positive. All the ionic concentration is expressed in ep. 55–85 % of the groundwater samples of the study area exhibit exchange of (Na^+ , K^+) in the water to Ca^{2+} , Mg^{2+} in rock by Scholler (1965) index to base exchange during all the seasons. It is calculated by the following expression:

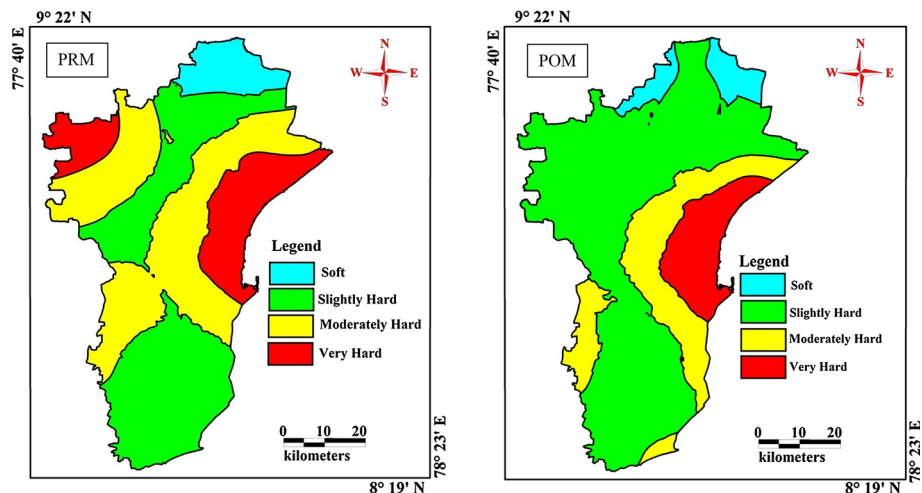


Fig. 23 Spatial distributions of TH during PRM and POM in the study area

$$\text{CAI 1} = [\text{Cl} - (\text{Na} + \text{K})/\text{Cl}]$$

$$\text{CAI 1} = [\text{Cl} - (\text{Na} + \text{K})/(\text{SO}_4 + \text{HCO}_3 + \text{CO}_3 + \text{NO}_3)]$$

Scholler classification (1967) for the dominance of anion exhibits that type I ($\text{rHCO}_3 > \text{rSO}_4$) is predominant in all the samples. Groundwater extracted from the study area for various purposes is transported by metallic pipes that may or may not be suitable for the transport. This fact is highlighted using corrosivity ratio (CR) proposed by Ryzner (1984). The formula for calculating CR is

$$\text{CR} = \{(\text{Cl}^-/35.5) + (\text{SO}_4^{2-}/96)\}/2(\text{HCO}_3^-) \times 100$$

It varies with seasons 90, and 61 % fall in safe category during PRM and POM, respectively, and the remaining percentage of the samples fall in unsafe category.

8 Conclusions

Groundwater in the Tuticorin District has been assessed for its quality and was found to be unsuitable for domestic and irrigation purposes during both seasons along coastal part of the study due to more saline water. The WQI of groundwater samples from the area was computed using an adjusted form of the Mitra and ASABE Member 1998 WQI equation. The analysis of the data suggests that 29 % shows “poor water,” 12 % shows “very poor water,” and 9 % indicates unsuitable for drinking purposes during PRM, and 20 % shows “poor water,” 6 % of samples shows “very poor water,” and remaining 7 % of the samples fall on unsuitable for drinking purposes during POM. Multivariate analysis of the hydrochemical parameters suggests that groundwater quality is attributed largely to the weathering of silicate and accessory minerals as well as seawater effects. This study finds that the major water type in the aquifers of western study area is the $\text{Ca}^{2+}\text{-Mg}^{2+}\text{-HCO}_3^-$ water type, which gradually degrades into more saline $\text{Na}^+\text{-Cl}^-\text{-SO}_4^{2-}$ water types toward the coast. High nitrate concentrations have been largely attributed to the effects of agricultural activities and domestic waste discharge in the area, and high fluoride with HCO_3^- concentration indicates weathering process and release of F^- from hydroxyl group of mineral, which confirmed by very low representation of pH central part of the study area. Factor score maps, showing the intensity of saltwater and salt pan activity is well noted along the coastal area, eastern part of the study area. The spatial distributions of the factor score show that quality of groundwater has been observed to decrease as salinity increases to astronomical levels toward the coast, largely due to seawater intrusion. It is also interesting to note that majority are unfit for drinking, irrigation, and domestic purpose during PRM compared to POM due to the dilution effect after rainfall.

References

- APHA. (1995). *Standard methods for the examination of water and waste water* (19th ed). Washington DC, USA: APHA.
- Appelo, C. A., & Postma, D. (1999). *Geochemistry, groundwater and pollution*. Rotterdam: Balkema.

- Avannavar, S. M., & Shrihari, S. (2008). Evaluation of water quality index for drinking purposes for river Netravathi, Mangalore, South India. *Environmental Monitoring and Assessment*, *143*, 279–290.
- Ayers, R. S., & Wascot, D. W. (1985). *Water quality for irrigation, FAO irrigation and drainage paper #20, Rev 1*. Rome: FAO.
- Balasubramanian, A. R., Thirugnana, S., Chellaswamy, R., & Radhakrishnan, V. (1993). *Numerical modeling for prediction and control of saltwater encroachment in the coastal aquifers of Tamil Nadu*. 21. Technical Report.
- Barbecot, F., Marlin, C., Gibert, E., & Dever, L. (2000). Hydrochemical and isotopic characterisation of the Bathonian and Bajocian coastal aquifer of the Caen area (northern France). *Applied Geochemistry*, *15*, 791–805.
- Briz-Kishore, B. H., & Murali, G. (1992). Factor analysis for revealing hydrochemical characteristics of a watershed. *Environmental Geology and Water Science*, *19*, 3–9.
- CGWB. (2009). *South Eastern Coastal Region*, District groundwater brochure, Tuticorin district, Tamil Nadu.
- Chadha, D. K. (1999). A proposed new diagram for geochemical classification of natural waters and interpretation of chemical data. *Hydrogeology Journal*, *7*, 431–439.
- Chapelle, F. H. (1983). Groundwater geochemistry and calcite cementation of the Aquia aquifer in south Maryland. *Water Resource Research*, *19*, 545–558.
- Chidambaram, S. (2000). Hydrogeochemical studies of groundwater in Periyar district, Tamil Nadu, India, unpublished Ph.D thesis, Department of Geology, Annamalai University.
- Chidambaram, S., Prasad, M. B. K., Manivannan, R., Karmegam, U., Singaraja, C., Anandhan, P., et al. (2013). *Environmental hydrogeochemistry and genesis of fluoride in groundwaters of Dindigul district*. Tamil Nadu: Environmental Earth Sciences. doi:10.1007/s12665-012-1741-9.
- Chidambaram, S., Ramanathan, A. L., Prasanna, M. V., Anandhan, P., Srinivasamoorthy, K., & Vasudeven, S. (2007). Identification of hydrogeochemically active regimes in groundwaters of Erode District, Tamil Nadu. A statistical approach. *Asian Journal of water, Environment and Pollution*, *5*, 93–102.
- Chidambaram, S., Senthil Kumar, G., Prasanna, M. V., John Peter, A., Ramanathan, A. L., & Srinivasamoorthy, K. (2009). A study on the hydrogeology and hydrogeochemistry of groundwater from different depths in a coastal aquifer: Annamalai Nagar, Tamil Nadu, India. *Journal of Environmental Geology*, *57*(1), 59–73.
- Chivas, A. R., Andrew, A. S., Lyons, W. B., Bird, M. I., & Donnelly, T. H. (1991). Isotopic constraints on the origin of salts in Australian playas. 1. Sulphur. *Palaeogeography, Palaeoclimatology, Palaeoecology. Palaeoenvironments of Salt Lakes*, *84*, 309–332.
- Chowdhury, A. K., Gupta, S. (2011). Evaluation of water quality, hydro-geochemistry of confined and unconfined aquifers and irrigation water quality in Digha Coast of West Bengal, India (A case study). *International Journal of Environmental Sciences*, *2*(2), ISSN 0976-4402.
- Dalton, M. G., & Upchurch, S. B. (1978). Interpretation of hydrochemical facies by factor analysis. *Groundwater*, *16*, 228.
- Domenico, P. A., & Schwartz, W. (1990). *Physical and chemical hydrogeology* (p. 824). New York: John Wiley.
- Doneen, L. D. (1948). The quality of irrigation water. California Agriculture Department, *4*, 6–14.
- Doneen, L. D. (1954). Salinization of soil by salts in the irrigation water. *Transaction, American Geophysical Union*, *35*, 943–950.
- Elango, L., & Kannan, R. (2007). Rock–water interaction and its control on chemical composition of groundwater. Chap. 11. *Developments in Environmental Science*, *5*, 229–243.
- Emerson, W. W., & Bakker, A. C. (1973). The comparative effect of exchangeable Ca: Mg and Na on some soil physical properties of red brown earth soils. 2. The spontaneous dispersion of aggregates in water. *Australian Journal of Soil Research*, *11*, 151–152.
- Gangai, I. P. D., & Ramachandran, S. (2010). The role of spatial planning in coastal management: A case study of coast (India). *Land Use Policy*, *27*, 518–534.
- Gibbs, R. J. (1970). Mechanisms controlling world's water chemistry. *Science*, *170*, 1088–1090.
- Gupta, S. K., & Gupta, I. C. (1987). *Management of saline soils and waters* (p. 339). New Delhi: Oxford and IBH Publishing and Co.
- Jacks, G. (1973). Chemistry of ground water in a district in Southern India. *Journal of Hydrology*, *18*, 185–200.
- Jeen, S. K., Kim, J. M., Ko, K. S., Yum, B., & Chang, H. W. (2001). Hydrogeochemical characteristics of groundwater in a mid-western coastal aquifer system. Korea. *Geoscience Journal*, *5*, 339–348.
- Joshi, D. M., Kumar, A., & Agrawal, N. (2009). Assessment of the irrigation water quality of River Ganga in Haridwar District India. *Journal of Chemistry*, *2*(2), 285–292.

- Kanwar, J. S., & Chaudhry, M. L. (1968). Effect of Mg on the uptake of nutrients from the soil. *Journal of Research Punjab Agricultural University*, 3, 309–319.
- Kelly, W. P. (1963). Use of saline irrigation water. *Soil Science*, 95(4), 355–391.
- Khaska, M., Sallea, C. L. G. L., Lancelot, J., Team, A., Mohamad, A., Verdoux, P., et al. (2013). Origin of groundwater salinity (current seawater vs. saline deep water) in a coastal karst aquifer based on Sr and Cl isotopes. Case study of the La Clape massif (southern France). *Applied Geochemistry*, 37, 212–227.
- Khodapanah, L., Sulaiman, W. N. A., & Khodapanah, N. (2009). Groundwater quality assessment for different purposes in Eshtehard District, Tehran, Iran. *European Journal of Scientific Research*, 36(4), 543–553.
- Kim, J. H., Yum, B.-W., Kim, R.-H., Koh, D.-C., Cheong, T.-J., Lee, J., & Chang, H.-W. (2003). Application of cluster analysis for the hydrogeochemical factors of saline groundwater in Kimje, Korea. *Geosciences Journal*, 7(4), 313–322.
- Krauskopf, K. B. (1979). *Introduction to geochemistry*. New York: McGraw-Hill.
- Lambrakis, N., & Kallergis, G. (2005). Contribution to the study of Greek thermal springs: Hydrogeological and hydrochemical characteristics and origin of thermal waters. *Hydrogeology Journal*, 13(3), 506–521.
- Manikandan, S., Chidambaram, S., Ramanathan, A. L., Prasanna, M. V., Karmegam, U., Singaraja, C., et al. (2012). A study on the high fluoride concentration in the magnesium-rich waters of hard rock aquifer in Krishnagiri district, Tamil Nadu, India. *Arabian Journal of Geosciences*. doi:10.1007/s12517-012-0752-x.
- Mathess, G. (1982). *The properties of ground water* (1st ed.). New York: Wiley.
- Mishra, P. C., & Patel, R. K. (2001). Study of the pollution load in the drinking water of Rairangpur, a small tribal dominated town of North Orissa. *Indian Journal of Environment and Ecoplanning*, 5(2), 293–298.
- Mitra, B. K. & ASABE Member. (1998). Spatial and temporal variation of ground water quality in sand dune area of aomori prefecture in Japan.
- Mondal, N. C., Singh, V. S., & Rangarajan, R. (2009). Aquifer characteristics and its modeling around an industrial complex, Tamil Nadu, India: A case study. *Journal of Earth System Sciences*, 188(3), 231–244.
- Mondal, N. C., Singh, V. S., Saxena, V. K., & Prasad, R. K. (2008). Improvement of ground water quality due to fresh water ingress in Potharlanka Island, Krishna delta, India. *Environmental Geology*, 55(3), 595–603.
- Nanyaro, J. T., Aswathanarayana, U., Mungore, J. S., & Lahermo, P. W. (1984). A geochemical model for the abnormal fluoride concentrations in waters in parts of northern Tanzania. *Journal of African Earth Science*, 2, 129–140.
- Nurmi, P. A., Kukkonen, I., & Lahermo, P. W. (1988). Geochemistry and origin of saline groundwaters in the Fennoscandian Shield. *Applied Geochemistry*, 3(2), 185–203.
- Oinam, J. D., Ramanathan, A. L., & Singh, G. (2012). Geochemical and statistical evaluation of groundwater in Imphal and Thoubal district of Manipur, India. *Journal of Asian Earth Sciences*, 48, 136–149.
- Paliwal, K. V. (1972). Effect of gypsum application on the quality of irrigation waters. *The Madras Agricultural Journal*, 59, 646–647.
- Panagopoulos, G., Lamprakis, N., Tsolis-Katagas, P., & Papoulis, D. (2004). Cation exchange processes and human activities in unconfined aquifers. *Environmental Geology*, 46, 542–552.
- Piper, A. M. (1953). A graphic procedure I the geo-chemical interpretation of water analysis. USGS Groundwater Note no. 12.
- Prasanna, M. V., Chidambaram, S., & Srinivasamoorthy, K. (2010). Statistical analysis of the hydrogeochemical evolution of groundwater in hard and sedimentary aquifers system of Gadilam river basin, South India. *Journal of King Saud University Science*, 22(3), 133–145.
- Puri, A. N. (1949). *Soils—Their physical chemistry* (p. 550). New York: Rein-hold Publishing and Co.
- Raghunath, H. M. (1987). *Geochemical survey and water quality* (pp. 343–347). New Delhi: Groundwater Wiley eastern limited.
- Rao, SN. (1997). *Studies on water quality index in hard rock terrain of Guntur district, Andhra Pradesh, India* (pp. 129–134). National Seminar on Hydrology of Precambrian Terrains and hard rock areas.
- Rao, N. S., Rao, P. S., Reddy, G. V., Nagamani, M., Vidyasagar, G., & Satyanarayana, N. L. V. V. (2012). Chemical characteristics of groundwater and assessment of groundwater quality in Varaha River Basin, Visakhapatnam District, Andhra Pradesh, India. *Environmental Monitoring Assessment*, 184, 5189–5214. doi:10.1007/s10661-011-2333-y.
- Rasouli, F. S., & Masoudi, S. F. (2012). Simulation of the BNCT of brain tumors using MCNP code: Beam designing and dose evaluation. *Iranian Journal of Medical Physics*, 9(3), 183–192.
- Richard, L. A. (1954). Diagnosis and improvement of saline and alkali soils. *USDA Handbook*, 60, 160.

- Richter, B. C., & Kreitler, C. W. (1993). *Geochemical techniques for identifying sources of ground-water salinization*. Boca Raton: CRC Press. 258.
- Ryzner, J. W. (1984). A New index for determination amount of calcium carbonate scale formed by water. *Journal American Water Works Association*, 36, 472–486.
- Saleh, A., Al-Ruwih, F., & Shehata, M. (1999). Hydrogeochemical processes operating within the main aquifers of Kuwait. *Journal of Arid Environment*, 42, 195–209.
- Scholler, H. (1965). Qualitative evaluation of groundwater resources. In *Methods and techniques of groundwater investigations and development*. UNESCO, 54–83.
- Scholler, H. (1967). *Methods and techniques of ground water investigation and development*. Water Resources Series no: 33, UNESCO.
- Senthilkumar, G., Ramanathan, A. L., Nainwal, H. C., & Chidambaram, S. (2008). Evaluation on the hydrogeochemistry of groundwater using factor analysis in the Cuddalore coastal region, Tamil Nadu, India. *Indian Journal of Marine Science*, 37, 2.
- Singaraja, C. (2014). A study on the hydrogeochemistry of groundwater in Tuticorin district of Tamil Nadu, India. Unpublished Ph.D thesis, Department of Earth Sciences, Annamalai University.
- Singaraja, C. (2015). GIS-Based Suitability Measurement of Groundwater Resources for Irrigation in Thoothukudi District, Tamil Nadu, India. *Water Quality, Exposure and Health*. doi:10.1007/s12403-015-0159-5.
- Singaraja, C., Chidambaram, S., Prasanna, M. V., Paramaguru, P., Johnsonbabu, G., & Thilagavathi, R. (2012). A study on the behavior of the dissolved oxygen in the shallow coastal wells of Cuddalore District, Tamil Nadu, India. *Water Quality, Exposure and Health*, 4, 1–16. doi:10.1007/s12403-011-0058-3.
- Singaraja, C., Chidambaram, S., Anandhan, P., Prasanna, M. V., Thivya, C., Thilagavathi, R., & Sarathidasan, J. (2013a). Hydrochemistry of groundwater in a coastal region and its repercussion on quality, a case study—Thoothukudi district, Tamil Nadu, India. *Arabian Journal of Geoscience*,. doi:10.1007/s12517-012-0794-0.
- Singaraja, C., Chidambaram, S., Prasanna, M. V., Thivya, C., & Thilagavathi, R. (2013b). Statistical analysis of the hydrogeochemical evolution of groundwater in hard rock coastal aquifers of Thoothukudi district in Tamil Nadu, India. *Journal of Environmental Earth Science*,. doi:10.1007/s12665-013-2453-5.
- Singaraja, C., Chidambaram, S., Anandhan, P., Prasanna, M. V., Thivya, C., Thilagavathi, R., & Sarathidasan, J. (2014a). *Geochemical evaluation of fluoride contamination of groundwater in the Thoothukudi District of Tamil Nadu*. India: Applied Water Sciences. doi:10.1007/s13201-014-0157-y.
- Singaraja, C., Chidambaram, S., Anandhan, P., Prasanna, M. V., Thivya, C., & Thilagavathi, R. (2014b). A study on the status of saltwater intrusion in the coastal hard rock aquifer of South India. *Environment, Development and Sustainability*,. doi:10.1007/s10668-014-9554-5.
- Singh, D. F. (1992). Studies on the water quality index of some major rivers of Pune, Maharashtra. *Proceedings of the Academy of Environmental Biology*, 1(1), 61–66.
- Singh, A., Mondal, K., Suresh Kumar, G. C., Singh, T. B., Tewary, B. K., & Sinha, A. (2008). Major ion chemistry, weathering processes and water quality assessment in upper catchment of Damodar River basin, India. *Environmental Geology*, 54, 745–758.
- Smith, S. J., Andres, R., Conception, E., & Lurz, J. (2004). *Sulfur Dioxide Emissions. 1850–2000* (Joint Global Change Research Institute Report. PNNL-14537).
- Soundranayagam, J. P., Sivasubramanian, P., Chandrasekar, N., & Rajamanickem, G. V. (2009). Remote sensing and GIS application in urban expansion and its impact on sea water intrusion in Thoothukudi, Tamil Nadu. *Indian Journal of Landscape Systems and Ecological Studies*, 32(2), 1–10.
- Srinivasamoorthy, K., Chidambaram, M., Prasanna, M. V., Vasanthavigar, M., Peter, J., & Anandhan, P. (2008). Identification of major sources controlling groundwater chemistry from a hard rock terrain—A case study from Mettur taluk, Salem district, Tamil Nadu, India. *Journal of Earth System Science*, 117(1), 49–58.
- Stumm, W., & Morgan, J. J. (1996). *Aquatic chemistry* (p. 1022). New York: John Wiley and sons Inc.
- Szabolcs, I., & Darab, C. (1964). *The influence of irrigation water of high sodium carbonate content of soils*. In Proceedings of 8th international congress of ISSS, Trans, II: pp. 803–812.
- Teotia, S. P. S., Teotia, M., & Singh, R. K. (1981). Hydrogeochemical aspects of endemic skeletal fluorosis in India - an epidemiological study. *Fluoride*, 14, 69–74.
- Thilagavathi, R., Chidambaram, S., Thivya, C., Prasanna, M. V., Singaraja, C., Tirumalesh, K., & Pethaperumal, S. (2014). Delineation of natural and anthropogenic process controlling hydrogeochemistry of layered aquifer sequence. *Proceedings of the National Academy of Sciences, India, Section A: Physical Sciences*, 88(1), 95–108.

- Thiyya, C., Chidambaram, S., Singaraja, C., Thilagavathi, R., Prasanna, M. V., & Jainab, I. (2013a). A study on the significance of lithology in groundwater quality of Madurai district, Tamil Nadu (India). *Environment, Development and Sustainability*,. doi:[10.1007/s10668-013-9439-z](https://doi.org/10.1007/s10668-013-9439-z).
- Thiyya, C., Chidambaram, S., Thilagavathi, R., Prasanna, M. V., Singaraja, C., & Nepolian, M. (2013b). Identification of the geochemical processes in groundwater by factor analysis in hard rock aquifers of Madurai District. *South India. Arabian Journal of Geosciences*,. doi:[10.1007/s12517-013-1065-4](https://doi.org/10.1007/s12517-013-1065-4).
- Todd, D. K. (1959). Seawater intrusion in costal aquifers. *Transactions American Geophysical Union*, *34*, 749–754.
- Todd, D. K. (1980). *Ground water hydrology*. New York: Wiley. 535.
- Udayalaxmi, G., Himabindu, D., & Ramadass, G. (2010). Geochemical evaluation of groundwater quality in selected areas of Hyderabad, A.P., India. *Indian Journal of Science and Technology*, *3*, 5.
- USSL. (1954). Diagnosis and improvement of Saline and alkali soils. *USDA Handbook*, *60*, 147.
- Vandenbohede, A., Courtens, C., & William de Breuck, L. (2010). Fresh-salt water distribution in the central Belgian coastal plain: An update. *Geologica Belgica*, *11*(3), 163–172.
- Warner, N. R., Kresse, T. M., Hays, P. D., Down, A., Karr, J. D., Jacksona, R. B., & Vengosha, A. (2013). Geochemical and isotopic variations in shallow groundwater in areas of the Fayetteville Shale development, north-central Arkansas. *Applied Geochemistry*, *35*, 207–220.
- WHO. (2004). *Guidelines for drinking water quality recommendations* (Vol. 1, p. 515). Geneva: WHO.
- Wilcox, L. V. (1955). Classification and use of irrigation water. *United States Geological Department Agriculture*, *969*, 19.
- Yidana, S. M., Banoeng-Yakubo, B., & Akabzaa, T. M. (2010). Analysis of groundwater quality using multivariate and spatial analyses in the Keta basin, Ghana. *Journal of African Earth Sciences*, *58*, 220–234.